In Vivo Multi-Day Calcium Imaging of CA1 Hippocampus in Freely Moving Rats Reveals a High Preponderance of Place Cells with Consistent Place Fields

Hannah S Wirtshafter[1*], John F Disterhoft[1]

*Lead contact: hsw@northwestern.edu (HSW)

1. Department of Neuroscience, Northwestern University Feinberg School of Medicine, Chicago, IL, USA.

Abstract: Calcium imaging using GCaMP indicators and miniature microscopes has been used to image cellular populations during long timescales and in different task phases, as well as to determine neuronal circuit topology and organization. Because the hippocampus (HPC) is essential for tasks of memory, spatial navigation, and learning, calcium imaging of large populations of HPC neurons can provide new insight on cell changes over time during these tasks. All reported HPC in vivo calcium imaging experiments have been done in mouse. However, rats have many behavioral and physiological experimental advantages over mice. In this paper, we present the first (to our knowledge) in vivo calcium imaging from CA1 hippocampus in freely moving male rats. Using the UCLA Miniscope, we demonstrate that, in rat, hundreds of cells can be visualized and held across weeks. We show that calcium events in these cells are highly correlated with periods of movement, with few calcium events occurring during periods without movement. We additionally show that an extremely large percent of cells recorded during a navigational task are place cells (77.3±5.0%, surpassing the percent seen during mouse calcium imaging), and that these cells enable accurate decoding of animal position and can be held over days with consistent place fields in a consistent spatial map. A detailed protocol is included, and implications of these advancements on *in vivo* imaging and place field literature are discussed.

Significance statement:

In vivo calcium imaging in freely moving animals allows the visualization of cellular activity across days. In this paper, we present the first in vivo Ca2+ recording from CA1 hippocampus in freely moving rats. We demonstrate that hundreds of cells can be visualized and held across weeks, and that calcium activity corresponds to periods of movement. We show that a high percentage (77.3±5.0%) of imaged cells are place cells, and that these place cells enable accurate decoding and can be held stably over days with little change in field location. Because the hippocampus is essential for many tasks involving memory, navigation, and learning, imaging of large populations of HPC neurons can shed new insight on cellular activity changes and organization.

Introduction

The explosion in the use of *in vivo* calcium imaging has allowed the visualization of hundreds of identified neurons over long time periods (Grienberger and Konnerth, 2012a; Grienberger and Konnerth, 2012b; Rickgauer et al., 2014; Hamel et al., 2015; Resendez et al., 2016; Aharoni and Hoogland, 2019b; Aharoni et al., 2019; Zhou et al., 2019). Calcium (Ca2+) imaging using GCaMP calcium indicators and miniature microscopes has been used to image cellular populations during long timescales (Dombeck et al., 2010; Ziv et al., 2013; Cai et al., 2016; Sheintuch et al., 2017; Hainmueller and Bartos, 2018; Kinsky et al., 2020; Sheintuch et al., 2020) and in different task phases (Zhang and Li, 2018; Jimenez et al., 2020; Shuman et al., 2020), as well as to determine neuronal circuit topography and organization (Klaus et al., 2017; Wang et al., 2017; Guo et al., 2020; Shin et al., 2020).

The hippocampus (HPC) has been studied with cellular resolution using *in vivo* electrophysiology, but this technique does not allow the same cells to be definitively followed over days, nor does it allow the visualization of cellular organization within the structure (O'Keefe, 1976; Wilson and McNaughton, 1993; McEchron and Disterhoft, 1999; Leutgeb et al., 2004; Schimanski et al., 2013). *In vivo* calcium imaging is particularly well suited for imaging the rodent HPC, as the orientation of the horizontal cell layer permits imaging of large numbers of neurons with insertion of a 1mm diameter or smaller lens (Guo et al., 2020; Kinsky et al., 2020; Sheintuch et al., 2020; Stefanini et al., 2020a). Because the hippocampus is essential for many tasks involving memory (Scoville and Milner, 1957; Squire, 1992; Eichenbaum et al., 1999; Hasselmo and McClelland, 1999; Ferbinteanu and Shapiro, 2003; Ferbinteanu et al., 2006; Smith and Mizumori, 2006; Vann, 2013; Cai et al., 2016; Josselyn and Tonegawa, 2020), spatial navigation (Foster et al., 2000; Rosenzweig et al., 2003; McNaughton et al., 2006; Foster and Knierim, 2012; Moser et al., 2017; Avigan et al., 2020), and learning (Moyer et al., 1990; Chan et al., 2001; Ito et al., 2005; Andrzejewski and Ryals, 2016), Ca2+ imaging of large populations of HPC neurons can shed new insight on cell changes and organization over time during these tasks.

To our knowledge, all reports of hippocampal *in vivo* calcium imaging have been done in mouse (although calcium imaging has been used to visualize other structures in rat (Scott et al., 2018; Anner et al., 2020; Hart et al., 2020; Pritchard et al., 2021)). Using calcium imaging in rat hippocampus requires optimizing a number of methodological parameters, including aspiration and lens implantation techniques, to account for the increased thickness of the rat alveus compared to mouse which makes focusing on the CA1 cell layer difficult (Swanson, 2004; Routh et al., 2009; Franklin and Paxinos, 2013). However, rats have many basic experimental advantages over mice: First, rats are able to learn and perform more complex tasks than mice, and employ more advanced strategies, and are thus suited for a wider variety of behavioral experiments (Whishaw, 1995; Frick et al., 2000; Whishaw et al., 2001; Cressant et al., 2007; Rosenfeld and Ferguson, 2014; Hok et al., 2016). Second, compared to mouse physiology, rat physiology for a number of conditions and disorders (including addiction, aging, and schizophrenia, among others) more closely mirrors human physiology (Iannaccone and Jacob, 2009; Vengeliene et al., 2014; Ellenbroek and Youn, 2016; Carter et al., 2020). Third, rats are less stressed by handling than mice, thus introducing less variability in experimental procedures (Buerge and Weiss, 2004).

Rats are also an advantageous organism to use for calcium imaging: Due to their larger size, rats are able to support larger implants, including a wider diameter imaging lens, larger and heavier cameras that may be available in the future, and more combinations with electrophysiology implants. This advantage will thereby enable the recording of a greater number of cells (Voigts et al., 2013; Aharoni and Hoogland, 2019b; Voigts et al., 2020). Additionally, rat hippocampal neurons are less excitable than those in mice (Routh et al., 2009; Hok et al., 2016), and rats are less prone to post-operative seizures than mice (Hunt et al., 2009, 2010; Bolkvadze and Pitkanen, 2012). Rats may therefore, compared to mice, be at a decreased risk of the seizures (and potentially to cell death) seen in mice after prolonged GCaMP expression (Tian et al., 2009b; Grienberger and Konnerth, 2012b; Resendez et al., 2016; Steinmetz et al., 2017; Yang et al., 2018).

Although *in vivo* Ca2+ imaging would appear to hold substantial promise for the study of hippocampus in freely moving rats, there is currently no direct evidence that it will work in this system. To our knowledge, there are no published studies employing *in vivo* Ca2+ imaging in rat hippocampus, likely partially due to the number of methodological changes necessary to adapt the technique from mice to rats. In this paper, we present reports of *in vivo* Ca2+ recording from CA1 hippocampus in freely moving rats. We demonstrate that hundreds of cells are reliably visualized and held across weeks using this technique, and that calcium activity corresponds to periods of movement. We show that during a navigational task involving retrieving food reward on a linear track, a uniquely high percentage (77.3±5.0%) of imaged cells are place cells (as compared to calcium imaging studies in mouse and electrophysiology studies in rat and mouse), and that these place cells enable accurate decoding and can be held stably over days with little change in field location. A detailed protocol for this technique, including notes on the numerous parameter changes needed to use Ca2+ in rats, is included in the Materials and Methods section, and implications of these advancements are discussed.

Materials and Methods

SUBJECT DETAILS

All procedures were performed within Northwestern Institutional Animal Care and Use Committee and NIH guidelines. Five male Fischer 344 x Brown Norway rats (275g to 325g) were sourced from National Institute on Aging colony at Charles River Laboratories, injected with AAV9-GCaMP7c, implanted with a 2mm GRIN lens and run on a linear maze (Figure 1). Animals were individually housed in an animal facility with a 12h light dark cycle.

METHOD DETAILS

GCaMP7c Injection and Lens Implantation

Rats were anesthetized with isoflurane (induction 4%, maintenance 1-2%). Following anesthesia, ear bars, and skull leveling, the skull was cleaned and a craniotomy site was marked above CA1 (stereotaxic coordinates Bregma AP -4.00mm, ML 3.00mm). The skull was scored around the craniotomy site using a razor blade to provide texture for future application of epoxy. A craniotomy was made with a 2mm trephine around the marked site and dura was removed with a bent 30 gauge needle. A Hamilton syringe (Gastight® 1700 Series Syringes, Hamilton, Model 1705 Small RN Syringe, Volume=50 μL, Point Style=3, Gauge=22s, Needle Length=50.8 mm) loaded with AAV9-GCaMP7c (obtained from Viogene Biosciences, packaged AAV9 of pGP-AAV-syn-jGCaMP7c-WPRE, titer $1.73*10^{13}$GC/mL) was lowered straight down to about 0.2mm past the CA1 cell layer (approximate coordinates Bregma AP -4.00mm, ML 3mm, DV 2.95mm relative to skull). 0.6uL of virus were injected over 12 minutes using an automated stereotaxic Injector. The syringe was then raised 0.2mm (Bregma AP -4.00mm, ML 3mm, DV 2.75mm) and another 0.6uL of virus were injected over 12 minutes (Figure 1a). The syringe was then left for 10 minutes before slowly raising to the skull.

We used a computerized stereotaxic injection system that allowed us to specify the coordinates of the injection. Due to the imprecision of craniotomies and imperfectly level skulls, often the initial injection at the specified sub-cortical coordinates did not fall

160 in the center of the craniotomy. To increase and maximize the spread of viral injection,
161 we completed a second injection. The process of lowering the syringe and doing two
162 injections was repeated so that the two syringe “lowering points” were evenly spread
163 throughout the craniotomy site. There were thus a total of four injections of 0.6uL each
164 (2.4uL total): two injections per each brain entrance site, each at different depths
165 (Figure 1a).

166 Following injection, four skull screws were screwed into the skull: one rostral to
167 bregma above the same hemisphere as the craniotomy, two between bregma and
168 lambda on the hemisphere opposite the craniotomy, and one behind lambda on the
169 hemisphere with the craniotomy. Under a dissecting microscope, tissue from the
170 craniotomy was then aspirated using a vacuum pump and 25 gauge needle that had
171 been previously blunted using a Dremel drill. Tissue was quickly aspirated until the start
172 of horizontal striations could be seen in the craniotomy hole. Care was then taken to
173 “level” the hole and make sure aspiration was at an even depth. The horizontal
174 striations of the corpus callosum were then carefully and slowly aspirated until the
175 vertical striations of the alveus were visible in the entirety of the craniotomy hole (Figure
176 1b). If the aspiration hole was bleeding, a small twisted piece of gel foam was inserted
177 into the hole for approximately five minutes and then removed.

178 *Notes differentiating this method from mouse Ca2+ imaging: We found the best*
179 *AAV for expression in rats was AAV9. Because of rat’s lower seizure threshold and,*
180 *anecdotally noted, lower GCaMP expression than in mice, four injection sites appear*
181 *both necessary and sufficient for ideal GCaMP expression. The injection volumes are*
182 *much larger than those used in mice (Ziv et al., 2013; Cai et al., 2016), which is made*
183 *possible due to the larger hippocampal area and the technique of injecting below the*
184 *CA1 cell layer, instead of on it. Unlike in mice, where just the cortex or most dorsal part*
185 *of the corpus callosum is aspirated (Cai et al., 2016; Schoenfeld et al., 2021), it is*
186 *important that the entire corpus callosum be completely aspirated in order to get very*
187 *close to the alveus.*

188 A 2mm GRIN lens (obtained from Go!Foton, CLH lens, 2.00mm diameter, 0.448
189 pitch, working distance 0.30mm, 550nm wavelength) was then held on the end of a

190 pipette using suction from the vacuum pump. The pipette was placed in the stereotaxic
191 instrument which was zeroed with the bottom of the lens on bregma. The lens was then
192 moved to the center of the craniotomy and lowered to a depth of approximately 3mm
193 from skull surface. The lens was then fixed in place with UV curing epoxy and the
194 vacuum pump was turned off and the pipette holding the lens removed. The epoxied
195 lens was then secured to the skull screws using dental acrylic. Animals were then given
196 buprenorphine (0.05mg/kg) and 20mL saline, taken off anesthesia, and allowed to
197 recover in a clean cage placed upon a heat pad.

198 *Notes differentiating this method from mouse Ca2+ imaging: A much larger lens*
199 *(2mm diameter as opposed to 0.5mm or 1.0mm diameter) lens can be used in rats due*
200 *to their larger size. Of high importance: in order to be as close to the CA1 layer as*
201 *possible, the lens is inserted further down (about .5mm) lower than the cell layer. This*
202 *serves, presumably, to temporarily compress the alveus to make sure the alveus is*
203 *pressed against the grin lens; this allows for in focus imaging of the CA1. We saw no*
204 *permanent compression of the CA1 cell layer (Figure 1C) or any behavioral deficits that*
205 *are associated with HPC compression (Shim et al., 2003; Chen et al., 2017). We had*
206 *zero visualization of cells unless the lens was deeply inserted. Additionally, unlike in*
207 *mouse implantation surgeries, we did not have success using meloxicam after surgery*
208 *as it appeared to cause excessive bleeding around the lens.*

209 Four to six weeks after surgery, animals were again anesthetized with isoflurane
210 and checked for cells expressing GCaMP. If expression was seen, the animal's lens
211 was base-plated. The baseplate was attached using UV-curing epoxy and dental
212 acrylic.

213 *Notes differentiating this method from mouse Ca2+ imaging: During base plating,*
214 *it gets progressively harder to see cells the longer the animal is under anesthesia.*
215 *Additionally, while a few cells will appear to be bright circles in the captured image, cells*
216 *do not appear to be flashing at all while the rat is under isoflurane, even after a tail pinch*
217 *or loud noise (techniques often used to incite a calcium burst during mouse base*
218 *plating). We recommend focusing on the bright, not flashing cells while base plating.*
219 *The entire field of view should become progressively brighter as the animal wakes up.*

We recommend not imaging for experiments within 24 hours of isoflurane exposure and base plating.

Behavioral Training

Prior to training, animals were food deprived to 85% body weight and maintained at this weight throughout the experiment. Implanted animals were trained on a 2.64m Med Associates linear track with pellet dispensers at either end. Animals learned to run back and forth between the sides of the track and received a grain pellet at alternate ends. Each pellet received was considered a trial. The fasted animals were able to achieve over 120 trials in 30 minutes. (Animal were fed after daily training to maintain weight.) Six sessions were selected for analysis for each animal, with first and last recorded sessions automatically included. When not being run, animals were housed in individual cages with a 12hr light- 12hr dark light cycle.

Six sessions from each animal were selection for analysis. Although each animal was run for at least seven sessions, occasionally an animal would refuse to run or run slowly (often the day following a run with a lot of pellets received). For the animal run the least number of times, only six sessions exceeded 50 trials per run. For consistency across analysis, we therefore selected the six sessions with the most trials to analyze from each animal. On average, the four animals ran 100.3+-33.1 trials per session, with the individual animals averaging 94.7+-35.3, 85.5+24.0, 114.5+-19.8, and 106.2+-41.2 trials per session.

Because the runs with the most trials were selected for analysis, trials were not always consecutive. If the first analyzed session is considered day 1, the analyzed sessions were as follows for each animal (as numbered by days on a calendar; animals were not necessarily run every day due to scheduling and equipment troubleshooting):

Animal 1: Days 1, 2, 3, 7, 8, 9 *(run across 9 days)*

Animal 2: Days 1, 2, 6, 7, 9, 13 *(run across 13 days)*

Animal 3: Days: 1, 2, 11, 14, 15, 16 *(run across 16 days)*

Animal 4: Days: 1, 2, 10, 14, 15, 16 *(run across 16 days)*

250 **Calcium Imaging**

251 One photon calcium imaging was done using UCLA V4 Miniscopes (Silva, 2017;
252 Aharoni and Hoogland, 2019a), assembled with standard lens configurations (two 3mm
253 diameter, 6mm FL achromat lens used in the objective module and one 4 mm diameter,
254 10mm FL achromat lens used in the emission module). We tested Ca2+ recording when
255 one of the objective module lenses was replaced by a 3mm diameter, 9mm FL
256 achromat lens, but no improvement in cell visualization was noted. Gain was set at high
257 and Miniscope LED intensity varied between 10 and 38.

258 *Notes differentiating this method from mouse Ca2+ imaging: Base fluorescence*
259 *appears lower in rats as compared to mice. While we have been advised that, using*
260 *Miniscopes, gain can often be on "low" for mouse imaging, we found it necessary to*
261 *have gain on "high" to visualize the highest number of cells.*

262

263 **GCaMP Visualization in Slice and Immunohistochemical Processing of Tissue**
264 **Sections**

265 Following conclusion of the study, animals were anesthetized and perfused with
266 PBS then 10% formalin. The brain was then sliced into 60 micron coronal sections. For
267 visualization as seen in Figure 1c, sections were mounted, let dry, and coverslipped
268 with Vectashield. Sections were then imaged with a confocal microscope.

269 For GCaMP and PV+ visualization in Figure 1d, all solutions were prepared in
270 phosphate buffered saline (PBS) containing 0.05% sodium azide and 2% normal
271 donkey serum. Free-floating sections were rinsed in PBS three times for a total of at
272 least 30 min between incubation steps. Tissue sections were sequentially placed in (1)
273 0.2% Triton X-100, 90 min; (2) mouse monoclonal anti-parvalbumin 2000X (Millipore),
274 48 hours; (3) rabbit anti-GFP 2000X,(AbCam), 24 hours; (4) biotinylated goat anti-rabbit
275 serum 200X (Jackson Immunochemicals), 90 min; (5) a cocktail containing Cy3
276 conjugated donkey anti-mouse serum 200x (Jackson Immunochemicals) and FITC
277 conjugated avidin 200x (Jackson), 90 min. Sections were coverslipped with a 9:1
278 mixture of glycerine and PBS containing 0.2% p-phenylenediamine and examined with
279 a confocal microscope.

QUANTIFICATION AND STATISTICAL ANALYSIS

Means are expressed as mean ± the standard deviation. Overall averages are computed by finding average per animal then averaging those values. All analysis code is available at https://github.com/hsw28/ca_imaging.

Position and speed analysis

Position was sampled by an overhead camera at 30Hz. Position tracking was done post-recording using Bonsai (Lopes et al., 2015). Speed was determined by taking the hypotenuse of the coordinates of the point one before and one after the time point of interest. Speed was then smoothed using a Gaussian kernel of 1s and speed was converted from pixels/s to cm/s.

Video pre-processing

Videos were recorded with Miniscope software at 15 frames/second and 752 by 480 pixels. All video processing was done using the Matlab-based CIATAH software (Ahanonu, 2018; Corder et al., 2019) and processing files are available at https://github.com/hsw28/ca_imaging/ . Videos were down sampled in space (3x using bi-linear interpolation) and time (2x). The video was normalized by subtracting the mean value of each frame from the frame. Each frame was then spatially filtered (normalized) using a bandpass FFT filter (70-100cycles/pixel). The video was then motion corrected to a chosen reference frame using TurboReg (Thevenaz et al., 1998). Videos were then converted to relative florescence (dF/F_0), where F_0 was the mean over the entire video.

Cell identification

Cells were first automatically identified using the Matlab-based CIATAH software (Ahanonu, 2018; Corder et al., 2019), using the CNMF-E method (Zhou et al., 2018).

Processing files are available at https://github.com/hsw28/ca_imaging/ . Images were filtered with a gaussian kernel of width 3 pixels. Neuron diameter was set at a pixel size of 13. The threshold for merging neurons was set at a calcium trace correlation of 0.65, and neurons were merged if their distances were smaller than 2 pixels and they had highly correlated spatial shapes (correlation>0.8) and small temporal correlations (correlation <0.4).

All cells identified using CNMF-E were then scored as neurons or not by a human scorer. Scoring was also done within the Matlab-based CIATAH software (Ahanonu, 2018; Corder et al., 2019) in a Matlab GUI. Human scoring was done while visualizing an activity trace, average Ca2+ waveform, a cropped movie montage of the candidate cell's Ca2+ events, and a maximum projection of all cells on which the candidate cell was highlighted. The relative fluorescence ($\Delta F/F_0$) local maxima of each identified cell were considered calcium event times.

Place cell identification and spiking characteristics

Place cells were identified using two criteria. First, cells must have a mean firing rate greater than 0.01Hz during periods of movement (>12cm/s) (Wirtshafter and Wilson, 2019, 2020). Second, the mutual information (MI) computed in either direction of travel must be greater than 95% of MI scores computed 500 times from shuffled cells (Kinsky et al., 2018). To compute MI, the track was divided lengthwise into 4cm bins, the firing rate of each cell and the occupancy of the animal were found for each bin. Rate and occupancy were smoothed with a 2cm Gaussian kernel. Mutual information was computed during periods of movement in each direction of travel as follows (Olypher et al., 2003; Kinsky et al., 2018; Wirtshafter and Wilson, 2020):

$$P_s = calcium\ event\ probability\ in\ each\ bin$$

$$P_o = occupancy\ probability\ at\ each\ bin$$

$$p = \frac{P_s}{P_o}$$

$$M_s = \sum P_s$$

$$M_o = \sum P_o$$

$$MI = \sum p * \log_2(\frac{p}{M_s * M_o})$$

Place field location was determined by the location of maximum firing rate after binning position into 4cm bins. Speed modulation for individual cells was determined by computing average event rate when the animal was moving <=5cm/s and >=12cm/s; a cell was considered speed modulated if the rate at >=12cm/s was larger. At the population level, speed modulation was determined by examining population event rate versus speed. Cross correlations between speed and event rate were computed by binning speed and rate into 100ms bins.

Position decoding

Position was decoded using all recorded cells in a session and was decoded for times when the rat was moving (velocity>12cm/s). The track was split in 10cm segments and the time window of decoding was 0.5 seconds with non-overlapping time bins. Decoding was done using Bayesian decoding (Zhang et al., 1998).

$x = positions, f_i(x) = average\ firing\ rate\ per\ second\ for\ cell\ N\ at\ position\ X$

$n = calcium\ events\ per\ cell, n_i = number\ of\ events\ in\ time\ window$

$N = total\ number\ of\ cells$

$t = time\ window\ of\ decoding$

$C(t,n) = normalization\ factor\ for\ probabilities\ to\ equal\ 1$

$P(x|n) = odds\ of\ being\ at\ position\ x\ giving\ calcium\ events\ n$

$$P(x|n) = C(t,n)\left(\prod_{i=1}^{N} f_i(x)^{n_i}\right)\exp\left(-t\sum_{i=1}^{N} f_i(x)\right)$$

Accuracy decoding was determined by randomly shuffling firing per position bins and re-decoding. The difference between actual and decoded position was then determined per time bin and compared to decoded shuffled data.

366 **Validation across days and within session**

367 Validation was done using the Matlab-based CIATAH software (Ahanonu, 2018;
368 Corder et al., 2019). Videos underwent 3 rounds of registration comprised of Turboreg
369 image rotation (Thevenaz et al., 1998). An image binarization threshold of 40% of the
370 images' maximum value was used to remove background noise and axons and
371 dendrites. A distance threshold of a maximum of 5 pixels was used to match cells
372 across sessions, with a minimum 2-D correlation coefficient of 0.5. All sessions were
373 aligned to the fourth recording session.

374 .

375

376

377 **Results**

378 To initiate Ca2+ imaging, we injected AAV9-Syn-GCaMP7c below the CA1 cell
379 layer in five male Fischer 344 x Brown Norway rats (Figure 1a, see Materials and
380 Methods) (Nathanson et al., 2009). After injection, in the same surgery, cortex and
381 corpus collosum were aspirated through a craniotomy until the alveus was clearly visible
382 (Figure 1b, see Materials and Methods). A 2mm diameter GRIN lens was inserted into
383 the craniotomy and cemented in place. Three animals were checked for GCaMP
384 expression four weeks after surgery, and all three animals showed expression and were
385 subsequently affixed with a base plate to secure the position of the Miniscope. The
386 other two animals were checked six weeks after surgery and showed expression and
387 were base plated. After the completion of the experiment, animals were sacrificed and
388 expression of GCaMP in CA1 pyramidal cells was verified with microscopy (Figure 1c).
389 Although contributions of interneurons cannot be ruled out, antibody staining for
390 parvalbumin positive (PV+) interneurons revealed that these cells constituted only a
391 small proportion of GCaMP cells in the stratum pyramidale (Figure 1d), consistent with
392 observations that <5% of cells in the pyramidal layer are interneurons (Aika et al.,
393 1994). GCaMP expression also appeared to be primarily limited to pyramidal cells in the
394 cell layer.

395 Animals were then food deprived to 85% body weight and trained on a 2.64m
396 linear track (Figure 1e). Animals were rewarded with grain pellets on alternating ends of
397 the linear track and quickly learned to run back and forth on the track. A visit to one
398 reward well signified a trial. Animals were run for a minimum of 30 minutes or 50 trials,
399 whichever came later, with total track time not to exceed one hour per session. Cells
400 were recorded for 7 days for one animal, 11 days for one animal, and 16 days for two
401 animals (n=4 rats, one of the five animals was eliminated when the implant was lost).

402 The six sessions with the most trials run were analyzed from each animal
403 (average trials run = 100.3±33.1, see Materials and Methods), with first and last
404 recorded sessions automatically included; sessions were not always consecutive (see
405 Materials and Methods). These sessions were analyzed for cellular activity using the
406 CNMF-E method implemented by the CIATAH software package (Ahanonu, 2018; Zhou

et al., 2018; Corder et al., 2019) (See Materials and Methods). A total of 5761 neurons were recorded over the 24 sessions, with a maximum of 428 cells from a single session (mean of 239.6±90.0 cells) (Figure 2a-d). The number of cells recorded from each animal across sessions was relatively constant (Figure 2c).

We then determined average calcium events/s across animals to be 0.090+-0.019 events/s, with individual animals averaging 0.084+-0.024, 0.074+-0.026, 0.085+-0.020, and 0.116+-0.032 events/second. (Figure 2D-E). Some difference in average calcium event rate could be accounted for by differences in the base line speeds of the animals: there was a significant positive correlation between the animal's average speed and the average events/s for each session ($F(22)=4.2$, $p=0.05$) (Figure 2F). Because speed is highly variable on a moment-to-moment basis, we also completed a cross-correlation between event rate and animal speed. In every session, we saw a positive cross-correlation between the animal's speed and the number of calcium events across the population. The average cross-correlation at a lag of 0s was 1.8+-0.08, although the average maximum cross-correlation was 0.2 +-0.7 at an average lag of +0.47+-0.54s, indicating that calcium events reliably followed changes in speed, as opposed to vice versa (Figure 2G).

Significantly, calcium activity appeared to be heavily modulated by the animal's activity, with periods of higher activity when the animal was running rather than stationary on the track (Figure 3). The biggest contributor to a change in event rate was transition from no movement to movement, with very few events occurring during periods of no movement (Figure 3C).

We then determined if there were place cells on any of the trials. A cell was considered to be a place cell if the mutual information (MI) computed in either direction of travel was greater than 95% of MI scores computed 500 times after shuffling the times of the calcium events that occur when the animal is moving (Ziv et al., 2013; Kinsky et al., 2018). Based on this criterion all trials contained place cells (Figure 3a). An average of 77.3±5.0%, of all cells recorded on the track were place cells (Figure 3), with individual rat averages at 71.6±10.6%, 77.3±1.2%, 76.4±9.5%, and 83.7±7.1%. We additionally determined the percentage of place cells if we only analyzed cells that had

437 an average calcium events rate of greater than 0.01hz (Stefanini et al., 2020a). This
438 additional criterion yielded an even higher percentage of place cells, with 88.3±4.4% of
439 these cells being classified as place cells. (Figure 3a).
440 We extended these results using an additional criterion previously used to
441 determine the percentage of place cells using calcium imaging (Stefanini et al., 2020a).
442 We determined the percentage of cells that would be place cells if the mutual
443 information value exceeded the mean plus three standard deviations of a shuffled
444 distribution. Using this criterion, we found that 64.3+-5.1 percent of all cells were place
445 cells, with individual animals at 59.5+-12.0%, 65.5+-2.3%, 61.2+-14%, and 71.0+-
446 12.1%. If we applied the 0.01hz threshold for cell inclusion to this group, 73.4+-4.3% of
447 cells were place cells, with individual animals at 68.0+-11.8%, 77.6+-5.6%, 77.0+-14.6%
448 and 76.0+-13.0%.
449 We wished to further investigate the properties of these place cells and to
450 confirm that cells were increasing their firing rate in place fields as is typical for
451 pyramidal cells; as opposed to interneurons that mark spatial location by a substantial
452 decrease in firing (Ego-Stengel and Wilson, 2007; Wilent and Nitz, 2007; Dombeck et
453 al., 2010)). We examined the place cells' maximum event rate during movement
454 (presumably occurring in the place field) with their average firing rate during movement.
455 The mean maximum rate was 0.15events/s, and the mean average rate was
456 0.02events/s. On average, cells increased firing 7.4x from their average firing rate
457 during movement to their maximum firing rate (Figure 4D). We next determined if speed
458 modulation occurred in the cells which display place fields. We compared whether
459 speed-modulated neurons increased their in-field firing rate as much as non-speed-
460 modulated neurons. We found no significant difference in firing rate increases between
461 speed-modulated and non-modulated neurons (t-test (4023)=0.7102, $p>0.05$), nor were
462 the distributions of increases different (KS-test $p>0.05$): both speed-modulated and non-
463 modulated cells increased their firing rates, on average, >7x from baseline at the center
464 of their place fields.
465 We then aimed to determine whether place cell firing was sufficient to decode the
466 position of the animal. We split the track in 10cm segments and used Bayesian

467 decoding to determine the position of the animal in non-overlapping 0.5 second
468 increments (Zhang et al., 1998). We found that the best positional decoding was
469 accurate to a median error of 4.3cm (1.6% of the 2.64m track). Across all animals,
470 accuracy ranged from a median of 4.3cm to 13.6cm (decoding errors were below 10cm
471 in 23 sessions and above 10cm in one session) with a median error of 5.9cm (Figure
472 5a). To confirm that decoding accuracy was better than chance we shuffled firing rate
473 per position bins and, using the shuffled data, decoded position. Median error for
474 shuffled data ranged from 59.1cm to 77.6cm, which was significantly worse than non-
475 shuffled data (Kruskal-Wallis test, $x^2(47)= 35.3$, $p=2.9*10^{-9}$) (Figure 5b).
476 We then aimed to determine if the same cells could be held over the duration of
477 our recordings (six recording sessions, spanning 7, 11, or 16 days). 40% of the cells
478 imaged on day one of the 7-day session were also present on day seven. Of the rat run
479 for 11 days, 31% of the cells present on day one were also present on day eleven. For
480 the two rats run 16 days, 28% and 50% of cells, respectively, that were present on day
481 one were also present on day sixteen. Across all four animals, cells that were imaged
482 on day one of recording had, on average, a 72±6% chance of being imaged on at least
483 one subsequent day of recording (Figure 6A). (Of note, while the camera was placed in
484 the same approximate position each day, thus allowing landmarks (such as blood
485 vessels) to be followed throughout the study, we did not attempt to perfectly align
486 landmarks or focal planes across days; instead recordings each day were made to
487 optimize total cell number in each day as proof of method.)
488 We then looked to determine how often a cell appeared in each session. Across
489 all cells, 59.4+-5.4% of cells were visible in only one session, 19.9+-2.4 were visible in
490 two, 11.2+-1.5 in three, 6.3+-0.8 in four, 2.3+-1.3 in five, and 1.0+-0.9 were in all six
491 sessions (Figure 6B). We then looked at place cells that were repeated across
492 sessions. As stated, 22.6+-4.3% of cells did not have place cells in any session. Of the
493 77.4% of cells that did have place fields, 61.0+-5.7% (47.2% of total cells) had fields in
494 only one session, 20.6+-2.0 (15.9% of total) had fields in two sessions, 10.8+-2.4%
495 (8.3% of total) had fields in three sessions, 5.1+-0.7% (4.9% of total) had fields in four
496 sessions, 2.0+-1.4% (1.5% of total) had fields in five sessions, and 0.5+-0.5 (0.4%of

497 total) had fields in all six sessions (Figure 6C). Place cell recurrence was not statistically
498 different from the recurrence of all cells (paired t-test(5)=$2.04*10^{-15}$, p=1).
499 We then determined the recurrence probability of a cell based on the number of
500 days apart the recording took place (Figure 6D). Three of our animals had relatively
501 consistent recurrence probabilities, while one animal (animal 3) was highly variable.
502 Going back to the recordings, we saw that recordings from this animal came from two
503 different focal planes, causing the recording of two different cell populations. Excluding
504 this animal, there was a modest trend across days for a decreasing recurrence
505 probability, with the probability of a cell reoccurring decreasing by 0.43% per day
506 separating the recording periods (Figure 6E).
507 We then determined whether a cell's place field remained in the same location
508 during days when the place cell reoccurred. We found that, across all days of recording,
509 the mean standard deviation of place field locations was about 36cm (~13% of track
510 length), with the individual animals at 39cm, 36cm, 32cm, and 37cm. We compared
511 these distances with distances if place field locations were shuffled, and we repeated
512 shuffling 500 times. All four animals had a smaller deviation between fields than would
513 be expected by chance ($p<0.05$ for all animals). Between individual days (including
514 nonadjacent days), the change in field distance was highly variable at 65cm+-71cm,
515 with a median of 40cm and a large concentration of values around 0cm (Figure 6F).
516 Although fields across days were more consistent than would have been
517 expected by random chance, we had not yet determined whether the animal had a
518 consistent map across all recording days (Ziv et al., 2013), or if it switched between
519 multiple maps (Sheintuch et al., 2020). To determine this, we compared place field
520 location for cells in a session against the place field locations of the same cells in
521 another session. To do this, for each cell, we plotted the location of the place field for
522 that session against the place field location of the same cell for another session. We did
523 this comparison for every cell that had a place field in more than one session. If place
524 field mapping was similar from session to session, we would expect the plotted field
525 locations of one session to have a strong positive correlation with the locations from
526 another session. Of the pairs of sessions that had more than 10 place cells shared

527 between sessions (57 out of 60 total session pairs—15 session pairs for rat 1, 15 for rat
528 2, 14 for rat 3, and 13 for rat 4), 53 of these pairs (93%) had a significant positive
529 correlation (f-test, $p<0.05$) between the place field locations, with no evidence of
530 switching between maps across days (Figure 6G). We found that correlations between
531 field locations did not decay as a function of the number of days between sessions
532 (Figure 6H).
533
534
535 **Discussion**
536
537 In this manuscript, we have demonstrated calcium imaging recordings can be
538 performed in the CA1 region of the hippocampus in freely moving rats. These
539 recordings can capture hundreds of cells in a single recording session, including a high
540 number and percentage of place cells sufficient to decode the animal's position to within
541 centimeters of accuracy, and that place cell field location is consistent across days.
542 Calcium imaging in rat will allow for more behaviorally complex and translational
543 experiments than have been done in mouse.
544
545 **Measuring Spatial Content**
546 We chose to use mutual information as the measure of spatial content for
547 multiple reasons: First, it has precedence for use in both calcium imaging (Ziv et al.,
548 2013; Meshulam et al., 2017; Kinsky et al., 2018; Kinsky et al., 2020; Stefanini et al.,
549 2020a) and electrophysiology studies (Jun et al., 2020) (Table 1). Second, threshold
550 measures commonly used in electrophysiology that depend on firing rate (such as "a
551 cell is a place cell if firing rate, as measured by electrophysiology, exceeds 2Hz for a
552 10cm area") (Rich et al., 2014) (Table 1) do not transfer well to calcium imaging
553 experiments as, using currently availably GCaMPs, calcium events are captured much
554 less frequently than spikes in electrophysiology (typically, ~0.02-0.06 events/s is the
555 mean rate observed during 1P calcium imaging, versus >0.5-1.5 spikes/s in
556 electrophysiology, a 25-fold difference, see Table 1). Third, other measures of

557 information content, such as bits/spike or bits/second (Table 1), tend to be highly
558 sensitive to changes in firing rate, including baseline firing rate (Souza et al., 2018), as
559 compared to mutual information. Specifically, cells with lower baseline firing rates are
560 favored to have higher baseline bits/spike or bits/second values (Souza et al., 2018;
561 Wirtshafter and Wilson, 2020), which makes it not a useful metric with which to compare
562 values from calcium imaging with data collected from electrophysiology. Additionally,
563 mutual information is advantageous in that it is a better predictor of decoding accuracy
564 than bits/spike and bits/second, and thus may better capture spatial informational
565 content (Souza et al., 2018). The criteria we used to identify place cells were as or more
566 stringent than previously used criteria in calcium imaging that identified a significantly
567 lower percentage of place fields (Table 1).
568 It is well established that pyramidal place cells increase their firing rate in their
569 place field, while interneurons express place specificity by decreasing firing rate. Given
570 that the majority of cells we observed displayed an increased rate of calcium events at
571 specific locations, it is reasonable to conclude that these were almost certainly
572 pyramidal cells in the stratum pyramidale. This conclusion is further supported by the
573 fact that many of the labeled cells displayed an obviously pyramidal morphology (Figure
574 1c), the infrequency of double labeling of GCaMP+ and PV+ cells (Figure 1d), and by
575 findings that only about 3% of cells in the stratum pyramidale are interneurons (Aika et
576 al., 1994). Additionally, GCaMP expression appears to be limited to pyramidal cells in
577 the cell layer, although it is unclear if this is a result of injection location or viral
578 specificity. As such, while it cannot be definitively determined if interneurons have
579 contributed to the observed effects, their numerical contribution would, at most, be very
580 small.
581
582 **The percentage of place cells in rat calcium imaging exceeds the percentage in**
583 **mouse calcium imaging**
584 Significantly, we found a higher percentage of cells were place cells in our
585 calcium imaging experiments in rats than those reported in mouse CA1 calcium imaging
586 experiments, even after the mice experiments were corrected for cells with low spiking

587 rates (Table 1). (The studies with mice reported 20-30% of imaged CA1 cells were
588 place cells, which is also substantially below most electrophysiology experiments (Ziv et
589 al., 2013; Stefanini et al., 2020b; Stefanini et al., 2020a)). Previous work has reported
590 that mouse place cells are less spatially tuned, contain less spatial information, and
591 have less stable place fields than in rat (Hok et al., 2016; Mou et al., 2018), so some of
592 the difference in place cell percent may be due to species differences in spatial
593 representations. However, there are also likely physiological differences between rats
594 and mice that affect the type of activity captured in calcium imaging recordings. CA1
595 cells in mice are more excitable than those in rat (Routh et al., 2009; Hok et al., 2016),
596 and prolonged GCaMP expression in mice has been shown to lead to cell
597 hyperexcitability, seizures, and even cell death (Tian et al., 2009b; Grienberger and
598 Konnerth, 2012b; Resendez et al., 2016; Steinmetz et al., 2017; Yang et al., 2018). The
599 higher baseline excitability of mouse cells, combined with a further increase in cellular
600 excitability after GCaMP expression may result in a lower threshold for cell firing and
601 less defined place fields, less stable fields, and, therefore, a seemingly lower number of
602 place cells compared to electrophysiology recordings (Hok et al., 2016). Because rats
603 have a lower baseline excitability, they may be less prone to these GCaMP effects,
604 although further slice electrophysiology work will need to be done to directly compare
605 the effect of GCaMP on mouse and rat neurons.
606 We considered that differences in calcium event rate between our data and other
607 studies might lead to the high percentage of place cells we saw in this work. On one
608 end of the spectrum, Stefanini et al 2020 found a particularly low percentage of place
609 cells (~4% of recorded cells in mouse CA1, using calcium imaging) and investigated
610 whether this might be a consequence of collecting many cells with low calcium event
611 rates. Their reported mean rate was 0.06+-0.04 events/s as recorded in mice in an open
612 field, consistent with 0.05-0.5 events/s in other calcium imaging experiments in mouse.
613 Even after eliminating cells with <0.1events/sec (a 10x less stringent criteria than we
614 used in Figure 3A), they still only found that 10-20% of cells were place cells (Stefanini
615 et al., 2020a). Conversely, Ziv 2013, who reported a high (for mouse) 20% of imaged
616 CA1 mouse cells were place cells, reported a higher mean event rate, at ~0.1-0.5

events/s (Ziv et al., 2013). Our results (0.090+-0.019 events/s, Figure 2D-E) are on the lower end of those reported in Ziv et al, and potentially consistent with the fact that rat neurons are somewhat less excitable than those in mice (Routh et al., 2009; Hok et al., 2016). Additionally, our very slightly lower event rate could be the result of less 'out of field' firing of place cells, which also tends to be more predominant in mice (Hok et al., 2016). However, our results are within the range of those reported in mouse imaging studies (Table 1), so differences in event rate are not a likely to be a major contributor to the place cell percentage we observed.

In addition to potentially allowing the recording of a higher number of place cells, the lower excitability of rat CA1 neurons, compared to mouse, also has other advantages. We saw no behavioral evidence of post-operative seizures in any of our implanted animals, and no behavioral or imaging evidence of seizures several months post viral injection and lens implementation. This is in contrast to calcium imaging experiments in mice, which frequently report that animals have to be removed from behavior or analysis due to the development of seizure activity (Steinmetz et al., 2017; Huang et al., 2021).

Differences in place cell findings between electrophysiology, intermediate early gene studies, and calcium imaging

The percentage of hippocampal CA1 cells found to be place cells using calcium recordings (77.3+-5.0%) was also very slightly above the upper range of findings from electrophysiological data in rats, which report that 35-75% of CA1 pyramidal cells recorded on a navigational task are place cells (the number varies widely depending on task parameters, with studies using a linear track task reporting the highest number of place cells) (Table 1) (Markus et al., 1994; Fenton et al., 2008; Wirtshafter and Wilson, 2020). There are multiple possible reasons related to recording technology as to why our calcium imaging experiments detected a higher percentage of place cells than traditional electrophysiology experiments: the difference likely resulted from electrophysiology capturing (as compared to calcium imaging) both a lower number of cells with active place fields detected (a smaller numerator) and a larger number of cells

647 without active place fields detected (a larger denominator). First, in electrophysiology
648 experiments with moveable electrodes (such as tetrodes), electrodes are typically
649 positioned while rats are inside a “sleep box” or other non-training apparatus until cells
650 are detected. The animal is then placed on a track for experimentation. This practice
651 optimizes cell detection for place cells that are active in the “sleep box” (both place cells
652 with fields in the sleep box, and place cells that are reactivated during ripples during
653 sleep), rather than cells that have place fields on the track. Adjusting and recording in a
654 sleep box therefore increases the number of total cells recorded that do not have fields
655 on the track and therefore reduce the place cell percentage. Because calcium imaging
656 uses a fixed lens location and images a large number of cells at once, recording is not
657 optimized for a particular environment. This may result in the recording of a higher
658 percentage of active place cells on the recording apparatus. (Due to logistical
659 constraints in this study, we did not complete any recording while the animal was not on
660 the track.) Second, while an effort is made in electrophysiology to discard times on the
661 track when the animal is not moving, and thus to remove corresponding spiking during
662 ripples, this removal is never perfectly done. The recording of ripples during
663 electrophysiology has two effects: the recording of cells that are being replayed on the
664 track but do not have place fields on the track and, second, the recording of ‘extra-field’
665 ripple spiking from cells with fields on the track. This ‘extra-field’ spiking can cause
666 place fields to seem less defined, and cause corresponding distortion of measures of
667 spatial information, such as mutual information and bits/spike. This, in turn, may cause
668 these cells not to be classified as place cells. Conversely, in calcium imaging, very few
669 to no calcium events are picked up during periods of no movement (see later in
670 discussion, figure 3), so both of these issues (increasing the count of cells without fields
671 on the track, and the distortion of spatial information for place cells) are avoided. Third,
672 while current GCaMPs, such as the GCaMP7c used in this study, have improved single
673 spike resolution compared to past GCaMPs, they still fall short of the single spike
674 resolution of electrophysiology (Tian et al., 2009a; Chen et al., 2013; Podor et al.,
675 2015a; Podor et al., 2015b; Shemesh et al., 2020). This property of calcium indicators
676 causes individual spikes, such as those that may occur on the track outside a cell’s

677 place field, to be missed, therefore biasing calcium imaging towards fast cell activity that
678 only occurs in the confines of a place field. Calcium imaging therefore, again, results in
679 potentially higher spatial information metrics as compared to electrophysiology, which
680 may cause the identification of more place cells. Finally, compared to electrophysiology,
681 calcium imaging provides additional characteristics (cell shape, size, and brightness) by
682 which to separate adjacent or nearby cells. Because conflation of multiple cells in
683 electrophysiology may disguise place fields and disrupt place field measurements (such
684 as mutual information or bits per spike), the additional resolution afforded by calcium
685 imaging may allow for more accurate place cell differentiation and identification.
686 Similar to electrophysiology and in contrast to intermediate early gene (IEG)
687 studies, calcium imaging is biased towards capturing cells active in an environment and
688 not the total cellular population. Additionally, as discussed above, due to limits on single
689 spike resolution, calcium imaging may be picking up even fewer cells with infrequent
690 spiking compared to electrophysiology. Thus, this bias of calcium imaging toward
691 detecting only active cells yields a higher percentage of place cells than intermediate
692 early gene studies that estimate a total of 30-40% of cells to be active in any given
693 environment (table 1) (Guzowski et al., 1999; Witharana et al., 2016).
694
695 **1P calcium imaging using GCAMP7c is movement responsive and minimally**
696 **activated when the animal is still**
697 Importantly, while calcium transients and events are correlated with action
698 potentials, they are far from a 1:1 correspondence and may capture more or less
699 information than electrophysiology (Huang et al., 2021). During our recording sessions,
700 we saw clear evidence that calcium event rate was correlated with periods of movement
701 (Figure 3). In electrophysiology experiments, place cell spiking is generally linearly
702 correlated with running speed (McNaughton et al., 1983; Huxter et al., 2003), and
703 significant spiking occurs during ripples when the animal is not moving (Ylinen et al.,
704 1995; Chrobak and Buzsaki, 1996; Csicsvari et al., 1999; Kudrimoti et al., 1999). Our
705 finding greatly differs from the patterns of spiking seen in electrophysiology data, as we
706 saw minimal calcium events during periods of no movement, with a pattern of

707 logarithmic growth of the number of calcium events as the animal began moving and
708 sped up (Figure 3C). Because the vast majority of CA1 pyramidal cells are speed and/or
709 ripple modulated, and we have imaged primarily pyramidal cells, this result is likely not
710 explainable by the population of cells that express GCaMP (Huxter et al., 2003). Our
711 result is consistent with calcium imaging experiments done in mice by Zhou et al., in
712 which more calcium events were seen during movement in an environment where food
713 reward could be obtained than during quiet wakefulness in a neutral box (Zhou et al.,
714 2019). In our experiment, periods of quiet wake were in the same environment (the
715 track) as periods of movement, which shows that changes in calcium event frequency
716 are related to movement and not to contextual associations. Zhou et al. posit that the
717 high amount of calcium activity that occurs during movement, but not during sharp wave
718 ripples in mouse, implicate calcium events in theta dependent processes, such as
719 memory encoding and planning (Buzsaki, 1989; Hasselmo et al., 2002; Hasselmo,
720 2005; Shirvalkar et al., 2010; Colgin, 2013; Wikenheiser and Redish, 2015; Zhou et al.,
721 2019; Wirtshafter and Wilson, 2021). It is possible, and consistent with slice data, that
722 NMDA receptors, which permit calcium influx, are minimally involved in cell spiking
723 during ripples, and the process is more heavily modulated by AMPA receptors, which do
724 not permit calcium influx (Maier et al., 2003; Colgin et al., 2004). There is also evidence
725 that activity during ripples can be visualized using 2-photon calcium imaging in mice
726 (Malvache et al., 2016; Grosmark et al., 2021), although we could not find any
727 experiments showing this activity using 1-photon imaging. It is therefore unclear
728 whether limits to imaging spiking activity during ripples is due to the imaging technique
729 or to the use of rats. Further work will be needed to determine if, in rat, frequent calcium
730 events are also unique to movement, as opposed to sharp wave ripples.
731
732 **Results show stable place cell identification and these cells have stable place**
733 **fields over days**
734 Our findings on cell activity over days were similar to and consistent with prior
735 results reported in mice. Prior work has reported that about 57% of cells are active in
736 only one or two sessions (Ziv et al., 2013); we found a higher proportion (59.4+-5.4% of

737 cells were visible in only one session, 19.9+-2.4 were visible in two) (Figure 6B), likely
738 because we worked to optimize cell count over precisely consistent focal planes. We
739 also reported that probability of a cell reoccurring decreased by 0.43% per day
740 separating recording sessions. This result was exactly consistent with prior results in
741 mouse that cell reoccurrence decreases from ~25% for sessions 5 days apart to ~15%
742 for sessions 30 days apart (25 days difference * 0.43 = ~10.8% change)(Figure 6E) (Ziv
743 et al., 2013). This potential cell turnover did not impact the accuracy of the
744 representation of the environment, as decoding accuracy was consistent throughout
745 sessions (Levy et al., 2021).
746 There are differing results regarding whether an environment has a single semi-
747 stable map (Ziv et al., 2013; Mau et al., 2018; Kinsky et al., 2020), or there are multiple
748 maps, involving the same cells, that code for a single environment (Sheintuch et al.,
749 2020). In this study, we only saw evidence of the former, as the vast majority of
750 sessions had cells with place fields correlated to previous sessions (Figure 6F) and
751 place field locations did not change as a function of the number of days between
752 sessions (Figure 6G). In other words, cell reoccurrence decreases across days, but
753 apparently when a cell does reoccur, its place field remains largely the same.
754
755 **Conclusion**
756 As previously mentioned, similarities between rat and human physiology, as well
757 as the increased capacity for complex tasks of learning and memory (Whishaw, 1995;
758 Frick et al., 2000; Whishaw et al., 2001; Cressant et al., 2007; Rosenfeld and Ferguson,
759 2014; Hok et al., 2016), position rats as a well-suited model organism for studying
760 hippocampal function, with several advantages over the mouse. Rats are advantageous
761 over mice in that, for many diseases and disorders, including those with substantial
762 hippocampal involvement, their physiology and behavior more closely mirrors that of
763 humans (Ellenbroek and Youn, 2016). For instance, 5-HT serotonin receptors, which
764 are prominent in the hippocampus and are implicated in a variety of disorders (including
765 mood and anxiety disorders, psychiatric disorders such as schizophrenia, addiction and
766 ADHD), are distributed in rats, but not in mice, in a similar pattern as seen in humans

767 (Hirst et al., 2003; Ellenbroek and Youn, 2016). Hippocampal neurogenesis, which is
768 believed to play an important role in learning, memory, and the treatment of depression,
769 is believed to follow a similar pattern in rats and humans, and is less pronounced in
770 mice (Snyder et al., 2009). In addition, both pharmacologic and behavioral responses to
771 addiction are more similar between rats and humans than mice and humans (Jupp et
772 al., 2013; Parker et al., 2014; Ellenbroek and Youn, 2016).
773 Having the ability to do calcium imaging in rat CA1 will allow increased research
774 into these disorders, as well as basic research in learning and memory. Because rats
775 are substantially larger than mice, they can support larger lens implants and cameras,
776 which may lead to the ability to record from thousands of hippocampal cells in a single
777 session during complex tasks. The ability to record a large number of cells across days
778 will allow research into cell firing changes in the hippocampus, which will provide insight
779 into more advanced learning and disease mechanisms that are difficult to understand
780 when only investigating mice. Additionally, the uniquely high percentage of recorded
781 place cells (>80% of recorded cells) makes CA1 calcium imaging in rats an ideal
782 method by which to study spatial navigation and learning over days, including
783 mechanisms behind memory consolidation, spatial remapping, and planning over time.
784
785
786
787
788

Figure captions

Figure 1: GCaMP is expressed in the CA1 cell layer of rat hippocampus

a. Diagram showing injection locations of AAV9-Syn-GCaMP7c, right below the CA1 cell layer. There are four total injection sites, with 0.6uL injected at each site. (CC = corpus callosum, DG = dentate gyrus)
b. Diagram showing level of aspiration in brain tissue. The entire corpus callosum is aspirated until the vertical striations of the alveus are visible.
c. GCaMP expression in the hippocampus, taken with a confocal microscope. The CA1 cell layer is labeled.
d. GCaMP appears to be highly localized to principal cells in the pyramidal cell layer. Left: GCaMP labeling. Center: Labeling for PV+ interneurons using immunohistochemistry (see methods). Right: Overlay of the two images.
e. Diagram of linear track. The animal would run back and forth between the two sides to receive a pellet reward

Figure 2: Hundreds of cells can be captured in a single Ca2+ imaging session

a. Examples of data from two (top and bottom rows) recording sessions. First column: example image from pre-processing. Second column: image post-processing (see materials and methods). Third column: all cell extractions, prior to manual cell sorting. Fourth column: post processing image overlayed with cell outlines identified after manual sorting.
b. Example traces from 15 cells taken during 124 seconds of calcium imaging.
c. Number of cells imaged per session for each rat. Dotted red line indicates the average for each animal.
d. Histogram showing average rate (events/second) for individual cells. Dotted red line indicates the average (0.090+-0.019 events/s)
e. The average calcium event rate (events/second) for individual rats (averages: 0.084+-0.024, 0.074+-0.026, 0.085+-0.020, and 0.116+-0.032 events/second)

818 f. Correlation of average calcium event rate with average animal running speed.
819 Average events per second in a session is positively correlated with the
820 animal's average speed in that session ($p<0.05$).
821 g. An example from one session for the cross-correlation at different lags
822 between the number of calcium events that occur in a second and the
823 animal's speed. In this example, the maximum cross correlation value at 0s
824 was about 0.33, and the maximum value occurred at about 0.1s. On average,
825 the cross-correlation at a lag of 0s was 1.8+-0.08, although the average
826 maximum cross-correlation was 0.2 +-0.7 at an average lag of +0.47+-0.54s,
827 indicating that calcium events reliably followed changes in speed, as opposed
828 to vice versa.
829
830 **Figure 3:** Calcium events are correlated with periods of movement
831 a. Raster plot of cell firing during linear track running. Top: the animal's speed.
832 Bottom: raster of peak calcium transients of 352 identified cells.
833 b. Graph showing an example of speed (plotted in black) overlayed with event rate
834 (in blue). Bottom panel is a zoom in of a smaller time period.
835 c. An example logarithmic correlation of animal speed against calcium events/
836 second.
837
838 **Figure 4:** A high percentage of place cells are recorded on the linear track using Ca2+
839 imaging
840 a. Graph showing the percentage of place cells per session for each rat (blue).
841 Analysis was repeated including only cells with a firing rate >0.01Hz during
842 movement (red). Dotted lines indicate the average for each animal.
843 b. Nine example place cells. A firing rate map in both directions of travel is
844 provided for each cell, with the top map corresponding with running to the
845 right, and the bottom map corresponding with running to the left. Note the
846 colorbar scales may be different for each direction of travel. The difference in
847 mutual information scores between the cell and the top 95% of shuffled data

848 (actual MI-shuffled MI) is indicated in the left corner. If the actual MI was
849 greater than 95% of shuffled data, the number is printed in bold white.
850 c. Distribution of directional mutual information scores after shuffling cells seen
851 in figure 3b. Event data was shuffled 500 times and the top 95% of mutual
852 information scores were determined from shuffled data (red dotted line). If the
853 actual mutual information score (green line) was greater than the upper 95%
854 MI score of shuffled data, the cell was considered to be a place cell.
855 d. Top left: Place field maximum event rate during movement (dotted red line
856 indicates average of 0.15events/s). Top right: average firing rate during
857 movement (red line is average at 0.02events/s). Bottom: Increase from
858 average to maximum rate (max/mean). On average, cells increased firing
859 7.4x from their average firing rate during movement to their maximum firing
860 rate (dotted red line indicates average)
861
862 **Figure 5:** Place cells are sufficient to decode the animal's position
863 a. Four decoding examples as the animal traverses the track. Black line
864 indicates the animal's actual position, with the stars indicated sample point.
865 The colored circles connected by the red line indicate decoded position. The
866 color of the circles indicates decoding certainty.
867 b. Same as A but decoding is using shuffled units. Decoding is much less
868 accurate using shuffled data.
869
870 **Figure 6:** Individual cells and their place fields can be maintained across sessions
871 a. Cells can be maintained across sessions weeks apart. Examples from two
872 animals of data taken on the first and final days of recording. Cells are color-
873 matched from the first to last day. Cells in gray represent cells with no
874 matches between the two days. Of note, while the camera was placed in the
875 same approximate position each day, thus allowing landmarks (such as blood
876 vessels) to be followed throughout the study, we did not attempt to perfectly

877 align landmarks or focal planes across days; instead recordings each day
878 were made to optimize total cell number in each day as proof of method.
879 **b.** Percent of cells that appeared in different numbers of sessions. Symbols
880 represent averages for individual animals. There was no significant difference
881 in distribution of values between animals (non-parametric k-sample
882 Anderson-Darling test, rank statistic: -1.48, $p>0.05$).
883 c. Percent of cells that had place fields in different numbers of sessions.
884 Symbols represent averages for individual animals. There was no significant
885 difference in distribution of values between animals (non-parametric k-sample
886 Anderson-Darling test, rank statistic: -1.59, $p>0.05$).
887 **d.** The recurrence probability of a cell based on the number of days between
888 recordings. Recordings from rat 3 were from found to be from two different
889 focal planes.
890 **e.** Average recurrence probability across days, excluding rat 3. For every day
891 passing, a cell has a 0.43% less chance of reoccurring.
892 **f.** Change in place field location between recording sessions. Included all
893 sessions recorded for an animal; sessions did not need to be adjacent.
894 g. A comparison of place field locations for one rat across all six recording
895 sessions (15 comparisons). For all 15 comparisons using this animal, place
896 field locations were highly correlated between the sessions. Each point
897 indicates the place field of a single cell identified in the two session indicated.
898 Red lines on the graphs indicate a $p<0.05$ using an F-test. Across all four
899 animals, we found field locations to be consistently correlated, with 93% of
900 session comparisons having a significantly positive correlation between place
901 field locations (f-test, $p<0.05$).
902 **h.** There was no correlation ($p>0.05$) between r2 value of place field correlations
903 and days elapsed between sessions.
904
905
906

Acknowledgements

We would like to thank all members of the Disterhoft lab, especially Matthew Oh, Craig Weiss, and Kent Park. We would also like to thank the Miniscope team, in particular Daniel Aharoni and Federico Sangiuliano Jimka. We additionally thank Biafra Ahanonu for assistance with CIATAH, Amy Christensen for providing advice during imaging setup, Drew Ames for consultation on figures, and David Wirtshafter for discussion, editing, and his assistance and expertise with immunohistochemistry.

Funding Disclosure

This work was supported by an NIA T32 (T32-AG020506/AG/NIA), an NIA R37 (R37-AG008796/AG/NIA) and an NINDS R01 (R01 NS113804/NS/NINDS).

Competing Interests

The authors declare no competing interests.

Related Manuscripts

Authors do not have a related or duplicate manuscript under consideration (or accepted) for publication elsewhere.

931

932

933

Citations

Ahanonu B (2018) CIAtah: a software package for analyzing one- and two-photon calcium imaging datasets. In, v1.0.0 Edition: Zenodo.

Aharoni D, Hoogland TM (2019a) Circuit investigations with open-source miniaturized microscopes: past, present and future. Frontiers in cellular neuroscience 13:141.

Aharoni D, Hoogland TM (2019b) Circuit Investigations With Open-Source Miniaturized Microscopes: Past, Present and Future. Frontiers in cellular neuroscience 13:141.

Aharoni D, Khakh BS, Silva AJ, Golshani P (2019) All the light that we can see: a new era in miniaturized microscopy. Nat Methods 16:11-13.

Aika Y, Ren JQ, Kosaka K, Kosaka T (1994) Quantitative analysis of GABA-like-immunoreactive and parvalbumin-containing neurons in the CA1 region of the rat hippocampus using a stereological method, the disector. Exp Brain Res 99:267-276.

Andrzejewski ME, Ryals C (2016) Dissociable hippocampal and amygdalar D1-like receptor contribution to discriminated Pavlovian conditioned approach learning. Behav Brain Res 299:111-121.

Anner P, Passecker J, Klausberger T, Dorffner G (2020) Ca2+ imaging of neurons in freely moving rats with automatic post hoc histological identification. Journal of neuroscience methods 341:108765.

Avigan PD, Cammack K, Shapiro ML (2020) Flexible spatial learning requires both the dorsal and ventral hippocampus and their functional interactions with the prefrontal cortex. Hippocampus 30:733-744.

Bolkvadze T, Pitkanen A (2012) Development of post-traumatic epilepsy after controlled cortical impact and lateral fluid-percussion-induced brain injury in the mouse. J Neurotrauma 29:789-812.

Buerge T, Weiss T (2004) Handling and Restraint. In: The Laboratory Mouse (Handbook of Experimental Animals) (Hedrich HJ, Bullock G, eds), pp 517-526: Elsevier.

Buzsaki G (1989) Two-stage model of memory trace formation: a role for "noisy" brain states. Neuroscience 31:551-570.

Cai DJ et al. (2016) A shared neural ensemble links distinct contextual memories encoded close in time. Nature 534:115-118.

Carter CS, Richardson A, Huffman DM, Austad S (2020) Bring Back the Rat! J Gerontol A Biol Sci Med Sci 75:405-415.

Chan KH, Morell JR, Jarrard LE, Davidson TL (2001) Reconsideration of the role of the hippocampus in learned inhibition. Behav Brain Res 119:111-130.

Chen LJ, Wang YJ, Chen JR, Tseng GF (2017) Hydrocephalus compacted cortex and hippocampus and altered their output neurons in association with spatial learning and memory deficits in rats. Brain Pathol 27:419-436.

Chen TW, Wardill TJ, Sun Y, Pulver SR, Renninger SL, Baohan A, Schreiter ER, Kerr RA, Orger MB, Jayaraman V, Looger LL, Svoboda K, Kim DS (2013) Ultrasensitive fluorescent proteins for imaging neuronal activity. Nature 499:295-300.

Chrobak JJ, Buzsaki G (1996) High-frequency oscillations in the output networks of the hippocampal-entorhinal axis of the freely behaving rat. J Neurosci 16:3056-3066.

977 Colgin LL (2013) Mechanisms and functions of theta rhythms. Annu Rev Neurosci 36:295-312.
978 Colgin LL, Kubota D, Jia Y, Rex CS, Lynch G (2004) Long-term potentiation is impaired in rat
979 hippocampal slices that produce spontaneous sharp waves. J Physiol 558:953-961.
980 Corder G, Ahanonu B, Grewe BF, Wang D, Schnitzer MJ, Scherrer G (2019) An amygdalar neural
981 ensemble that encodes the unpleasantness of pain. Science 363:276-281.
982 Cressant A, Besson M, Suarez S, Cormier A, Granon S (2007) Spatial learning in Long-Evans
983 Hooded rats and C57BL/6J mice: different strategies for different performance. Behav
984 Brain Res 177:22-29.
985 Csicsvari J, Hirase H, Czurko A, Mamiya A, Buzsaki G (1999) Fast network oscillations in the
986 hippocampal CA1 region of the behaving rat. J Neurosci 19:RC20.
987 Dombeck DA, Harvey CD, Tian L, Looger LL, Tank DW (2010) Functional imaging of hippocampal
988 place cells at cellular resolution during virtual navigation. Nat Neurosci 13:1433-1440.
989 Ego-Stengel V, Wilson MA (2007) Spatial selectivity and theta phase precession in CA1
990 interneurons. Hippocampus 17:161-174.
991 Eichenbaum H, Dudchenko P, Wood E, Shapiro M, Tanila H (1999) The hippocampus, memory,
992 and place cells: is it spatial memory or a memory space? Neuron 23:209-226.
993 Ellenbroek B, Youn J (2016) Rodent models in neuroscience research: is it a rat race? Dis Model
994 Mech 9:1079-1087.
995 Fenton AA, Kao H-Y, Neymotin SA, Olypher A, Vayntrub Y, Lytton WW, Ludvig N (2008)
996 Unmasking the CA1 ensemble place code by exposures to small and large environments:
997 more place cells and multiple, irregularly arranged, and expanded place fields in the
998 larger space. Journal of Neuroscience 28:11250-11262.
999 Ferbinteanu J, Shapiro ML (2003) Prospective and retrospective memory coding in the
1000 hippocampus. Neuron 40:1227-1239.
1001 Ferbinteanu J, Kennedy PJ, Shapiro ML (2006) Episodic memory—from brain to mind.
1002 Hippocampus 16:691-703.
1003 Foster DJ, Knierim JJ (2012) Sequence learning and the role of the hippocampus in rodent
1004 navigation. Curr Opin Neurobiol 22:294-300.
1005 Foster DJ, Morris RG, Dayan P (2000) A model of hippocampally dependent navigation, using
1006 the temporal difference learning rule. Hippocampus 10:1-16.
1007 Franklin KBJ, Paxinos G (2013) Paxinos and Franklin's The mouse brain in stereotaxic
1008 coordinates.
1009 Frick KM, Stillner ET, Berger-Sweeney J (2000) Mice are not little rats: species differences in a
1010 one-day water maze task. Neuroreport 11:3461-3465.
1011 Grienberger C, Konnerth A (2012a) Imaging calcium in neurons. Neuron 73:862-885.
1012 Grienberger C, Konnerth A (2012b) Imaging calcium in neurons. Neuron 73:862-885.
1013 Grosmark AD, Sparks FT, Davis MJ, Losonczy A (2021) Reactivation predicts the consolidation of
1014 unbiased long-term cognitive maps. Nat Neurosci 24:1574-1585.
1015 Guo W, Zhang JJ, Newman JP, Wilson MA (2020) Latent learning drives sleep-dependent
1016 plasticity in distinct CA1 subpopulations. bioRxiv:2020.2002.2027.967794.
1017 Guzowski JF, McNaughton BL, Barnes CA, Worley PF (1999) Environment-specific expression of
1018 the immediate-early gene Arc in hippocampal neuronal ensembles. Nat Neurosci
1019 2:1120-1124.

1020 Hainmueller T, Bartos M (2018) Parallel emergence of stable and dynamic memory engrams in
1021 the hippocampus. Nature 558:292-296.
1022 Hamel EJ, Grewe BF, Parker JG, Schnitzer MJ (2015) Cellular level brain imaging in behaving
1023 mammals: an engineering approach. Neuron 86:140-159.
1024 Hart EE, Blair GJ, O'Dell TJ, Blair HT, Izquierdo A (2020) Chemogenetic modulation and single-
1025 photon calcium imaging in anterior cingulate cortex reveal a mechanism for effort-based
1026 decisions. Journal of Neuroscience 40:5628-5643.
1027 Hasselmo ME (2005) What is the function of hippocampal theta rhythm?--Linking behavioral
1028 data to phasic properties of field potential and unit recording data. Hippocampus
1029 15:936-949.
1030 Hasselmo ME, McClelland JL (1999) Neural models of memory. Curr Opin Neurobiol 9:184-188.
1031 Hasselmo ME, Hay J, Ilyn M, Gorchetchnikov A (2002) Neuromodulation, theta rhythm and rat
1032 spatial navigation. Neural Netw 15:689-707.
1033 Hirst WD, Abrahamsen B, Blaney FE, Calver AR, Aloj L, Price GW, Medhurst AD (2003)
1034 Differences in the central nervous system distribution and pharmacology of the mouse
1035 5-hydroxytryptamine-6 receptor compared with rat and human receptors investigated
1036 by radioligand binding, site-directed mutagenesis, and molecular modeling. Molecular
1037 pharmacology 64:1295-1308.
1038 Hok V, Poucet B, Duvelle É, Save É, Sargolini F (2016) Spatial cognition in mice and rats:
1039 similarities and differences in brain and behavior. Wiley Interdisciplinary Reviews:
1040 Cognitive Science 7:406-421.
1041 Huang L, Ledochowitsch P, Knoblich U, Lecoq J, Murphy GJ, Reid RC, de Vries SE, Koch C, Zeng H,
1042 Buice MA (2021) Relationship between simultaneously recorded spiking activity and
1043 fluorescence signal in GCaMP6 transgenic mice. eLife 10:e51675.
1044 Hunt RF, Scheff SW, Smith BN (2009) Posttraumatic epilepsy after controlled cortical impact
1045 injury in mice. Exp Neurol 215:243-252.
1046 Hunt RF, Scheff SW, Smith BN (2010) Regionally localized recurrent excitation in the dentate
1047 gyrus of a cortical contusion model of posttraumatic epilepsy. J Neurophysiol 103:1490-
1048 1500.
1049 Huxter J, Burgess N, O'Keefe J (2003) Independent rate and temporal coding in hippocampal
1050 pyramidal cells. Nature 425:828-832.
1051 Iannaccone PM, Jacob HJ (2009) Rats! Dis Model Mech 2:206-210.
1052 Ito R, Everitt BJ, Robbins TW (2005) The hippocampus and appetitive Pavlovian conditioning:
1053 effects of excitotoxic hippocampal lesions on conditioned locomotor activity and
1054 autoshaping. Hippocampus 15:713-721.
1055 Jimenez JC, Berry JE, Lim SC, Ong SK, Kheirbek MA, Hen R (2020) Contextual fear memory
1056 retrieval by correlated ensembles of ventral CA1 neurons. Nature communications
1057 11:3492.
1058 Josselyn SA, Tonegawa S (2020) Memory engrams: Recalling the past and imagining the future.
1059 Science 367.
1060 Jun H, Bramian A, Soma S, Saito T, Saido TC, Igarashi KM (2020) Disrupted Place Cell Remapping
1061 and Impaired Grid Cells in a Knockin Model of Alzheimer's Disease. Neuron 107:1095-
1062 1112 e1096.

Jupp B, Caprioli D, Dalley JW (2013) Highly impulsive rats: modelling an endophenotype to determine the neurobiological, genetic and environmental mechanisms of addiction. Dis Model Mech 6:302-311.

Kinsky NR, Sullivan DW, Mau W, Hasselmo ME, Eichenbaum HB (2018) Hippocampal Place Fields Maintain a Coherent and Flexible Map across Long Timescales. Current biology : CB 28:3578-3588 e3576.

Kinsky NR, Mau W, Sullivan DW, Levy SJ, Ruesch EA, Hasselmo ME (2020) Trajectory-modulated hippocampal neurons persist throughout memory-guided navigation. Nature communications 11:2443.

Klaus A, Martins GJ, Paixao VB, Zhou P, Paninski L, Costa RM (2017) The Spatiotemporal Organization of the Striatum Encodes Action Space. Neuron 95:1171-1180 e1177.

Kudrimoti HS, Barnes CA, McNaughton BL (1999) Reactivation of hippocampal cell assemblies: effects of behavioral state, experience, and EEG dynamics. J Neurosci 19:4090-4101.

Leutgeb S, Leutgeb JK, Treves A, Moser MB, Moser EI (2004) Distinct ensemble codes in hippocampal areas CA3 and CA1. Science 305:1295-1298.

Levy SJ, Kinsky NR, Mau W, Sullivan DW, Hasselmo ME (2021) Hippocampal spatial memory representations in mice are heterogeneously stable. Hippocampus 31:244-260.

Lopes G, Bonacchi N, Frazao J, Neto JP, Atallah BV, Soares S, Moreira L, Matias S, Itskov PM, Correia PA, Medina RE, Calcaterra L, Dreosti E, Paton JJ, Kampff AR (2015) Bonsai: an event-based framework for processing and controlling data streams. Front Neuroinform 9:7.

Maier N, Nimmrich V, Draguhn A (2003) Cellular and network mechanisms underlying spontaneous sharp wave-ripple complexes in mouse hippocampal slices. J Physiol 550:873-887.

Malvache A, Reichinnek S, Villette V, Haimerl C, Cossart R (2016) Awake hippocampal reactivations project onto orthogonal neuronal assemblies. Science 353:1280-1283.

Markus EJ, Barnes CA, McNaughton BL, Gladden VL, Skaggs WE (1994) Spatial information content and reliability of hippocampal CA1 neurons: effects of visual input. Hippocampus 4:410-421.

Mau W, Sullivan DW, Kinsky NR, Hasselmo ME, Howard MW, Eichenbaum H (2018) The Same Hippocampal CA1 Population Simultaneously Codes Temporal Information over Multiple Timescales. Current biology : CB 28:1499-1508 e1494.

Maurer AP, Cowen SL, Burke SN, Barnes CA, McNaughton BL (2006) Organization of hippocampal cell assemblies based on theta phase precession. Hippocampus 16:785-794.

McEchron MD, Disterhoft JF (1999) Hippocampal encoding of non-spatial trace conditioning. Hippocampus 9:385-396.

McNaughton BL, Barnes CA, O'Keefe J (1983) The contributions of position, direction, and velocity to single unit activity in the hippocampus of freely-moving rats. Experimental brain research 52:41-49.

McNaughton BL, Battaglia FP, Jensen O, Moser EI, Moser MB (2006) Path integration and the neural basis of the 'cognitive map'. Nat Rev Neurosci 7:663-678.

Meshulam L, Gauthier JL, Brody CD, Tank DW, Bialek W (2017) Collective Behavior of Place and Non-place Neurons in the Hippocampal Network. Neuron 96:1178-1191 e1174.

1107 Moser EI, Moser M-B, McNaughton BL (2017) Spatial representation in the hippocampal
1108 formation: a history. Nature neuroscience 20:1448-1464.
1109 Mou X, Cheng J, Yu YS, Kee SE, Ji D (2018) Comparing mouse and rat hippocampal place cell
1110 activities and firing sequences in the same environments. Frontiers in cellular
1111 neuroscience 12:332.
1112 Moyer JR, Jr., Deyo RA, Disterhoft JF (1990) Hippocampectomy disrupts trace eye-blink
1113 conditioning in rabbits. Behav Neurosci 104:243-252.
1114 Nathanson JL, Yanagawa Y, Obata K, Callaway EM (2009) Preferential labeling of inhibitory and
1115 excitatory cortical neurons by endogenous tropism of adeno-associated virus and
1116 lentivirus vectors. Neuroscience 161:441-450.
1117 O'Keefe J (1976) Place units in the hippocampus of the freely moving rat. Exp Neurol 51:78-109.
1118 Olypher AV, Lansky P, Muller RU, Fenton AA (2003) Quantifying location-specific information in
1119 the discharge of rat hippocampal place cells. J Neurosci Methods 127:123-135.
1120 Parker CC, Chen H, Flagel SB, Geurts AM, Richards JB, Robinson TE, Woods LCS, Palmer AA
1121 (2014) Rats are the smart choice: rationale for a renewed focus on rats in behavioral
1122 genetics. Neuropharmacology 76:250-258.
1123 Podor B, Hu Y-l, Ohkura M, Nakai J, Croll R, Fine A (2015a) Comparison of genetically encoded
1124 calcium indicators for monitoring action potentials in mammalian brain by two-photon
1125 excitation fluorescence microscopy. Neurophotonics 2:021014.
1126 Podor B, Hu YL, Ohkura M, Nakai J, Croll R, Fine A (2015b) Comparison of genetically encoded
1127 calcium indicators for monitoring action potentials in mammalian brain by two-photon
1128 excitation fluorescence microscopy. Neurophotonics 2:021014.
1129 Pritchard A, Hornung R, Kramer PR (2021) Measuring calcium activity within individual neurons
1130 within the rat thalamus. MethodsX 8:101273.
1131 Resendez SL, Jennings JH, Ung RL, Namboodiri VM, Zhou ZC, Otis JM, Nomura H, McHenry JA,
1132 Kosyk O, Stuber GD (2016) Visualization of cortical, subcortical and deep brain neural
1133 circuit dynamics during naturalistic mammalian behavior with head-mounted
1134 microscopes and chronically implanted lenses. Nature protocols 11:566-597.
1135 Rich PD, Liaw HP, Lee AK (2014) Place cells. Large environments reveal the statistical structure
1136 governing hippocampal representations. Science 345:814-817.
1137 Rickgauer JP, Deisseroth K, Tank DW (2014) Simultaneous cellular-resolution optical
1138 perturbation and imaging of place cell firing fields. Nat Neurosci 17:1816-1824.
1139 Rosenfeld CS, Ferguson SA (2014) Barnes maze testing strategies with small and large rodent
1140 models. J Vis Exp:e51194.
1141 Rosenzweig ES, Redish AD, McNaughton BL, Barnes CA (2003) Hippocampal map realignment
1142 and spatial learning. Nature neuroscience 6:609-615.
1143 Routh BN, Johnston D, Harris K, Chitwood RA (2009) Anatomical and electrophysiological
1144 comparison of CA1 pyramidal neurons of the rat and mouse. Journal of neurophysiology
1145 102:2288-2302.
1146 Schimanski LA, Lipa P, Barnes CA (2013) Tracking the course of hippocampal representations
1147 during learning: when is the map required? J Neurosci 33:3094-3106.
1148 Schoenfeld G, Carta S, Rupprecht P, Ayaz A, Helmchen F (2021) In vivo calcium imaging of CA3
1149 pyramidal neuron populations in adult mouse hippocampus. eNeuro.

Scott BB, Thiberge SY, Guo C, Tervo DGR, Brody CD, Karpova AY, Tank DW (2018) Imaging cortical dynamics in GCaMP transgenic rats with a head-mounted widefield macroscope. Neuron 100:1045-1058. e1045.

Scoville WB, Milner B (1957) Loss of recent memory after bilateral hippocampal lesions. Journal of neurology, neurosurgery, and psychiatry 20:11-21.

Sheintuch L, Geva N, Baumer H, Rechavi Y, Rubin A, Ziv Y (2020) Multiple Maps of the Same Spatial Context Can Stably Coexist in the Mouse Hippocampus. Current biology : CB 30:1467-1476 e1466.

Sheintuch L, Rubin A, Brande-Eilat N, Geva N, Sadeh N, Pinchasof O, Ziv Y (2017) Tracking the Same Neurons across Multiple Days in Ca(2+) Imaging Data. Cell reports 21:1102-1115.

Shemesh OA et al. (2020) Precision Calcium Imaging of Dense Neural Populations via a Cell-Body-Targeted Calcium Indicator. Neuron 107:470-486 e411.

Shim I, Ha Y, Chung JY, Lee HJ, Yang KH, Chang JW (2003) Association of learning and memory impairments with changes in the septohippocampal cholinergic system in rats with kaolin-induced hydrocephalus. Neurosurgery 53:416-425; discussion 425.

Shin JH, Song M, Paik SB, Jung MW (2020) Spatial organization of functional clusters representing reward and movement information in the striatal direct and indirect pathways. Proc Natl Acad Sci U S A 117:27004-27015.

Shirvalkar PR, Rapp PR, Shapiro ML (2010) Bidirectional changes to hippocampal theta–gamma comodulation predict memory for recent spatial episodes. Proceedings of the National Academy of Sciences 107:7054-7059.

Shuman T et al. (2020) Breakdown of spatial coding and interneuron synchronization in epileptic mice. Nat Neurosci 23:229-238.

Silva AJ (2017) Miniaturized two-photon microscope: seeing clearer and deeper into the brain. Light: Science & Applications 6:e17104-e17104.

Smith DM, Mizumori SJ (2006) Hippocampal place cells, context, and episodic memory. Hippocampus 16:716-729.

Snyder JS, Choe JS, Clifford MA, Jeurling SI, Hurley P, Brown A, Kamhi JF, Cameron HA (2009) Adult-born hippocampal neurons are more numerous, faster maturing, and more involved in behavior in rats than in mice. Journal of Neuroscience 29:14484-14495.

Souza BC, Pavão R, Belchior H, Tort AB (2018) On information metrics for spatial coding. Neuroscience 375:62-73.

Squire LR (1992) Memory and the hippocampus: a synthesis from findings with rats, monkeys, and humans. Psychol Rev 99:195-231.

Stefanini F, Kushnir L, Jimenez JC, Jennings JH, Woods NI, Stuber GD, Kheirbek MA, Hen R, Fusi S (2020a) A Distributed Neural Code in the Dentate Gyrus and in CA1. Neuron 107:703-716 e704.

Stefanini F, Kushnir L, Jimenez JC, Jennings JH, Woods NI, Stuber GD, Kheirbek MA, Hen R, Fusi S (2020b) A distributed neural code in the dentate gyrus and in CA1. Neuron 107:703-716. e704.

Steinmetz NA et al. (2017) Aberrant Cortical Activity in Multiple GCaMP6-Expressing Transgenic Mouse Lines. eNeuro 4.

Swanson L (2004) Brain maps: structure of the rat brain: Gulf Professional Publishing.

Talbot ZN, Sparks FT, Dvorak D, Curran BM, Alarcon JM, Fenton AA (2018) Normal CA1 Place Fields but Discoordinated Network Discharge in a Fmr1-Null Mouse Model of Fragile X Syndrome. Neuron 97:684-697 e684.
Thevenaz P, Ruttimann UE, Unser M (1998) A pyramid approach to subpixel registration based on intensity. IEEE Trans Image Process 7:27-41.
Tian L, Hires SA, Mao T, Huber D, Chiappe ME, Chalasani SH, Petreanu L, Akerboom J, McKinney SA, Schreiter ER (2009a) Imaging neural activity in worms, flies and mice with improved GCaMP calcium indicators. Nature methods 6:875-881.
Tian L, Hires SA, Mao T, Huber D, Chiappe ME, Chalasani SH, Petreanu L, Akerboom J, McKinney SA, Schreiter ER, Bargmann CI, Jayaraman V, Svoboda K, Looger LL (2009b) Imaging neural activity in worms, flies and mice with improved GCaMP calcium indicators. Nat Methods 6:875-881.
Vann SD (2013) Dismantling the Papez circuit for memory in rats. eLife 2:e00736.
Vengeliene V, Bilbao A, Spanagel R (2014) The alcohol deprivation effect model for studying relapse behavior: a comparison between rats and mice. Alcohol 48:313-320.
Voigts J, Siegle JH, Pritchett DL, Moore CI (2013) The flexDrive: an ultra-light implant for optical control and highly parallel chronic recording of neuronal ensembles in freely moving mice. Front Syst Neurosci 7:8.
Voigts J, Newman JP, Wilson MA, Harnett MT (2020) An easy-to-assemble, robust, and lightweight drive implant for chronic tetrode recordings in freely moving animals. J Neural Eng 17:026044.
Wang X, Liu Y, Li X, Zhang Z, Yang H, Zhang Y, Williams PR, Alwahab NSA, Kapur K, Yu B, Zhang Y, Chen M, Ding H, Gerfen CR, Wang KH, He Z (2017) Deconstruction of Corticospinal Circuits for Goal-Directed Motor Skills. Cell 171:440-455 e414.
Whishaw IQ (1995) A comparison of rats and mice in a swimming pool place task and matching to place task: some surprising differences. Physiol Behav 58:687-693.
Whishaw IQ, Metz GA, Kolb B, Pellis SM (2001) Accelerated nervous system development contributes to behavioral efficiency in the laboratory mouse: a behavioral review and theoretical proposal. Developmental Psychobiology: The Journal of the International Society for Developmental Psychobiology 39:151-170.
Wikenheiser AM, Redish AD (2015) Hippocampal theta sequences reflect current goals. Nat Neurosci 18:289-294.
Wilent WB, Nitz DA (2007) Discrete place fields of hippocampal formation interneurons. J Neurophysiol 97:4152-4161.
Wilson MA, McNaughton BL (1993) Dynamics of the hippocampal ensemble code for space. Science 261:1055-1058.
Wirtshafter HS, Wilson MA (2019) Locomotor and Hippocampal Processing Converge in the Lateral Septum. Current biology : CB 29:3177-3192.
Wirtshafter HS, Wilson MA (2020) Differences in reward biased spatial representations in the lateral septum and hippocampus. eLife 9.
Wirtshafter HS, Wilson MA (2021) Lateral septum as a nexus for mood, motivation, and movement. Neurosci Biobehav Rev 126:544-559.
Witharana WK, Cardiff J, Chawla MK, Xie JY, Alme CB, Eckert M, Lapointe V, Demchuk A, Maurer AP, Trivedi V, Sutherland RJ, Guzowski JF, Barnes CA, McNaughton BL (2016)

Nonuniform allocation of hippocampal neurons to place fields across all hippocampal subfields. Hippocampus 26:1328-1344.

Yang Y, Liu N, He Y, Liu Y, Ge L, Zou L, Song S, Xiong W, Liu X (2018) Improved calcium sensor GCaMP-X overcomes the calcium channel perturbations induced by the calmodulin in GCaMP. Nature communications 9:1504.

Ylinen A, Bragin A, Nadasdy Z, Jando G, Szabo I, Sik A, Buzsaki G (1995) Sharp wave-associated high-frequency oscillation (200 Hz) in the intact hippocampus: network and intracellular mechanisms. J Neurosci 15:30-46.

Zhang K, Ginzburg I, McNaughton BL, Sejnowski TJ (1998) Interpreting neuronal population activity by reconstruction: unified framework with application to hippocampal place cells. J Neurophysiol 79:1017-1044.

Zhang X, Li B (2018) Population coding of valence in the basolateral amygdala. Nature communications 9:5195.

Zhou H, Neville KR, Goldstein N, Kabu S, Kausar N, Ye R, Nguyen TT, Gelwan N, Hyman BT, Gomperts SN (2019) Cholinergic modulation of hippocampal calcium activity across the sleep-wake cycle. eLife 8.

Zhou P, Resendez SL, Rodriguez-Romaguera J, Jimenez JC, Neufeld SQ, Giovannucci A, Friedrich J, Pnevmatikakis EA, Stuber GD, Hen R, Kheirbek MA, Sabatini BL, Kass RE, Paninski L (2018) Efficient and accurate extraction of in vivo calcium signals from microendoscopic video data. eLife 7.

Ziv Y, Burns LD, Cocker ED, Hamel EO, Ghosh KK, Kitch LJ, El Gamal A, Schnitzer MJ (2013) Long-term dynamics of CA1 hippocampal place codes. Nat Neurosci 16:264-266.

Table 1. Comparison of place cell findings in previous studies in mice and rats

Study	**Method**	**Species**	**Task**	**Mean spike rate or Ca event rate**	**% place cells**	**How place cells were determined**
Guzowski et al. 1999	IEG	Rat	Cylinder and platform exploration	NA	**38-39%**	ARC detection
Witharana et al. 2016	IEG	Rat	Environmental exposure and circular track	NA	**22-73%,** mean 33±18%	Homer1a and ARC detection
Talbot et al. 2018	Ephys	Mouse	Open field	1.14±0.12 spikes/s for all pyramidal cells 1.49±0.15 spikes/s for place cells 2.61 ± 0.2 spikes/s mean in-field rate	**47.8%**	overall discharge rate was 0.1-2 AP/s, the spatial coherence was >0.4, and the information content was >0.4 bits/spike
Jun et al. 2020	Ephys	Mouse	Open field and linear track	~0.8 spikes/s mean rate ~3.5 spikes/s maximum rate	**50%**	Mutual information >95% of shuffled data
Maurer et al. 2006	Ephys	Rat	Circular track	Not noted	**~43%** on smaller track **~68%** on larger track	place field has a single cycle (360%) phase precession
Wirtshafter and Wilson 2020	Ephys	Rat	Double sided T maze	~0-5hz in field	**75.2%** exceeded 0.8 bits/spike **63%** had at least one place field and exceeded bits/spike threshold	1) Bits/second >0.8 2) firing in a region must be greater than two standard deviations greater than the mean firing rate and place field area must be at least 15 cm long
Fenton et al. 2008	Ephys	Rat	Forage for food in cylinder and chamber	0.91-1.01 spikes/s depending on environment	**64%** in smaller cylinder **72%** in 6x larger chamber	cell coherence was >0.25 and information content was >0.5 bits/AP, and if the cell had at

				2-2.5 spikes/s mean in-field rate		least one place field.
Markus et al. 1994	Ephys	Rat	8 arm radial maze forced choice	0.56 spikes/s in young animals	**37%**	Bits/spike cutoff of 2.29
Rich et al. 2014	Ephys	Rat	48m long track	Up to ~0.7 spikes/s during running, highly correlated with # of place fields	**65%** at 48m (range 46-77%)	A place field was defined as >=15 contiguous cm of rate map in where firing rate > 2 Hz.
Meshulam et al. 2017	2p calcium imaging	Mouse	VR linear track	Not noted	**~30%,** range 28% to 41%.	Mutual information above 80% of shuffled
Ziv et al. 2013	1p calcium imaging	Mouse	Linear track	~0-0.5 events/s	**20%**	Mutual information above 95% of shuffled
Stefanini et al. 2020	1p calcium imaging	Mouse	Open field	0.06 ± 0.04 ev/s	MI mean+3σ: **~4%** for all cells **~10%** with 0.1ev/s cutoff >95% shuffled MI **~12%** for all cells **~22%** with 0.1ev/s cutoff	Mutual information > mean+3σ of the shuffled distribution. Also compared to mutual information above 95% of shuffled
Kinsky et al. 2018	1p calcium imaging	Mouse	Square and octagon tracks	Not noted	Unspecified	1) had >= 5 calcium transients during the session 2) Mutual information above 95% of shuffled
Kinsky et al. 2020	1p calcium imaging	Mouse	Continuous alternation	0.02-0.03 ev/s (mean ~40-50 events in ~30m session)	Unspecified	1) had >= 5 calcium transients during the session 2) Mutual information above 95% of shuffled

This work	1p calcium imaging	Rat	Linear track	0.02events/s during movement only 0.15events/s mean maximum in-field rate	>95% shuffled MI **77.3%** for all cells **88.3%** with 0.01ev/s cutoff MI mean+3σ: **64.3%** for all cells **73.4%** with 0.01ev/s cutoff	Mutual information above 95% of shuffled Also computed mutual information > mean+3σ of the shuffled distribution.

Figure 1

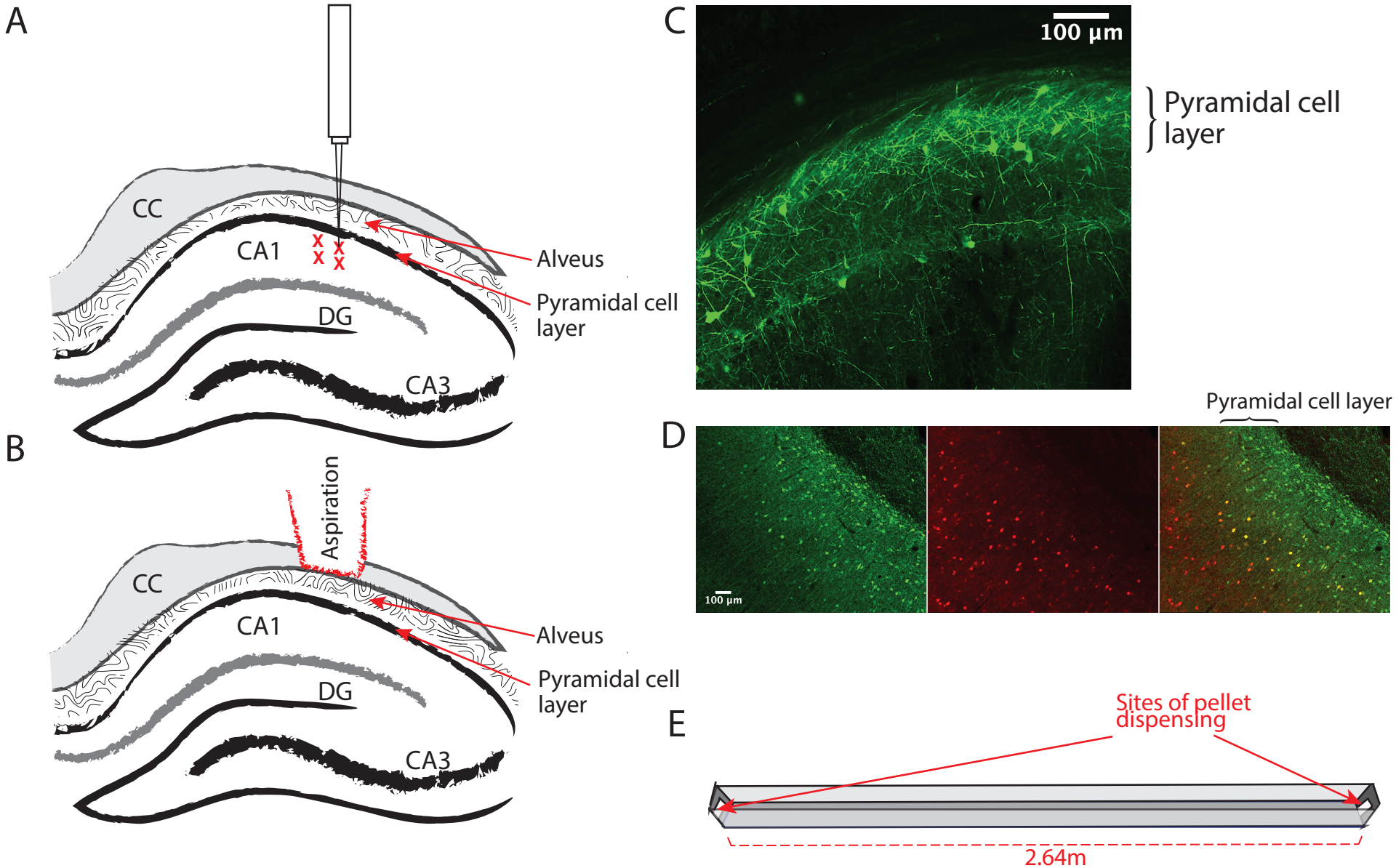
A
CC
CA1
DG
CA3
Alveus
Pyramidal cell layer
B
Aspiration
CC
CA1
DG
CA3
Alveus
Pyramidal cell layer
C
100 µm
Pyramidal cell layer
D
Pyramidal cell layer
100 µm
E
Sites of pellet dispensing
2.64m

Figure 2

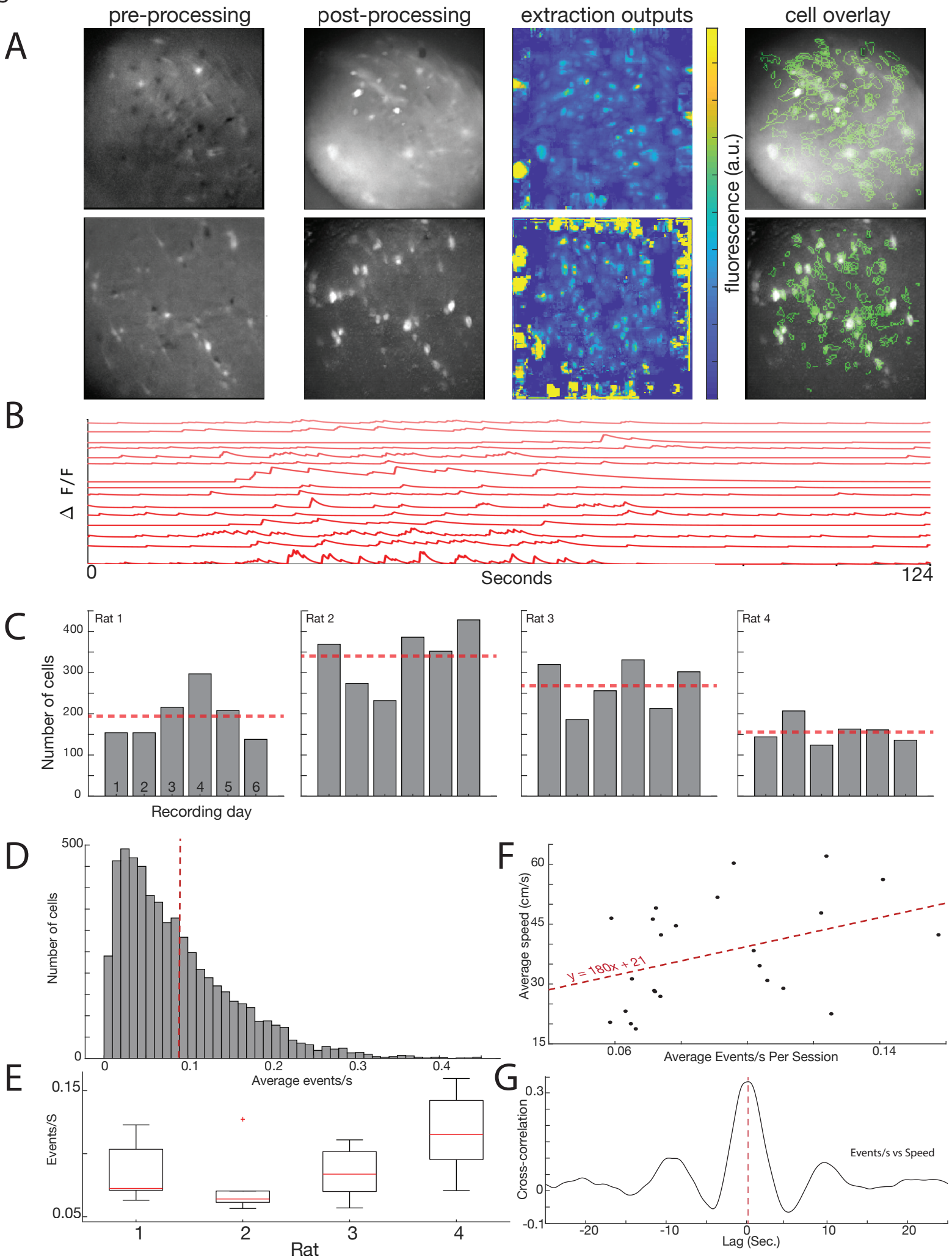
A
pre-processing
post-processing
extraction outputs
cell overlay
fluorescence (a.u.)
B
Δ F/F
0
Seconds
124
C
Rat 1
Rat 2
Rat 3
Rat 4
Number of cells
400
300
200
100
0
1
2
3
4
5
6
Recording day
D
500
Number of cells
0
0
0.1
0.2
0.3
0.4
Average events/s
E
0.15
0.05
Events/S
1
2
3
4
Rat
F
60
45
30
15
Average speed (cm/s)
y = 180x + 21
0.06
0.14
Average Events/s Per Session
G
0.3
0
-0.1
Cross-correlation
Events/s vs Speed
-20
-10
0
10
20
Lag (Sec.)

Figure 3

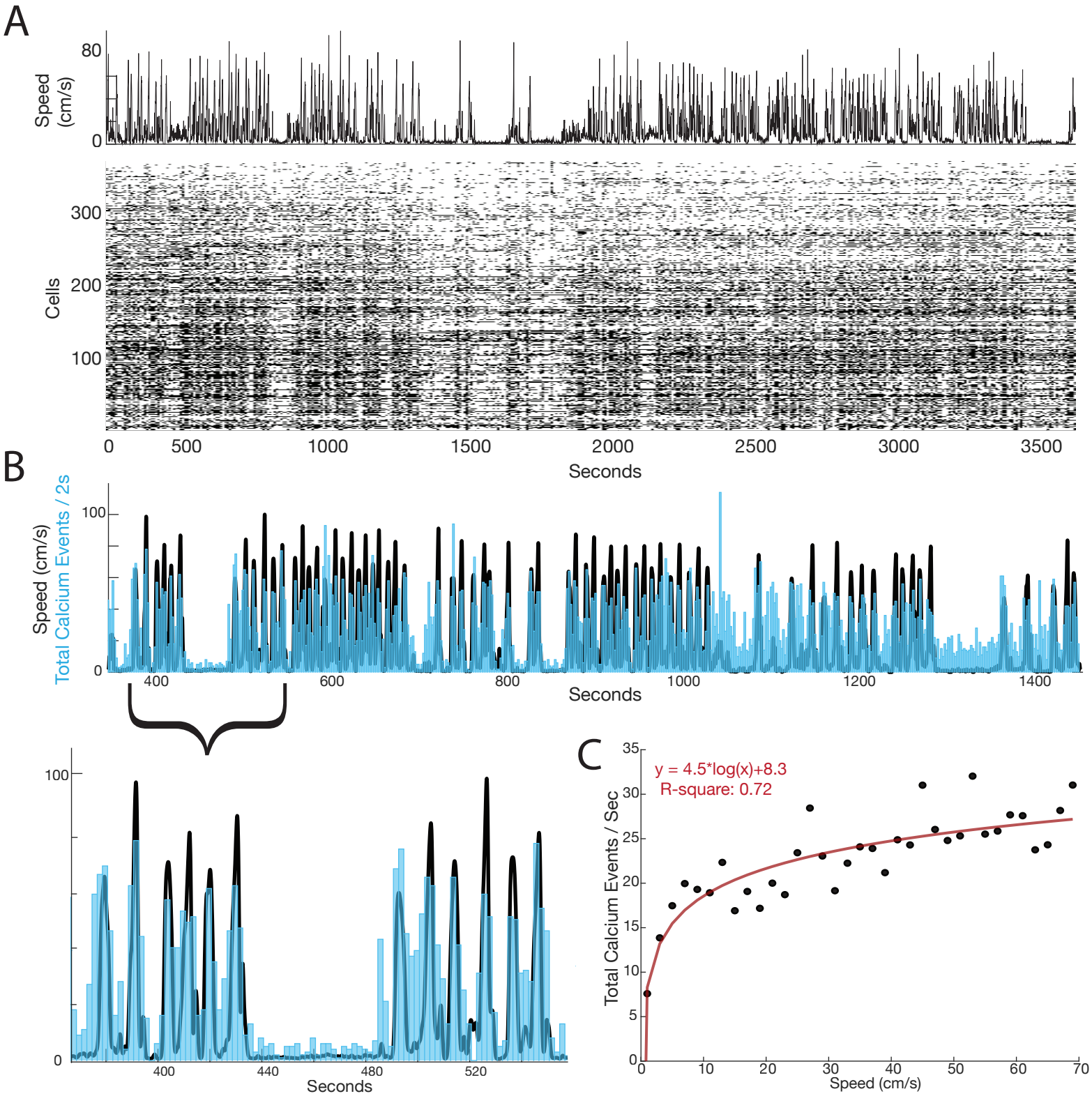
A
Speed (cm/s)
80
0
Cells
300
200
100
0
500
1000
1500
2000
2500
3000
3500
Seconds
B
Speed (cm/s)
Total Calcium Events / 2s
100
0
400
600
800
1000
1200
1400
Seconds
100
0
400
440
480
520
Seconds
C
y = 4.5*log(x)+8.3
R-square: 0.72
Total Calcium Events / Sec
35
30
25
20
15
10
5
0
0
10
20
30
40
50
60
70
Speed (cm/s)

Figure 4

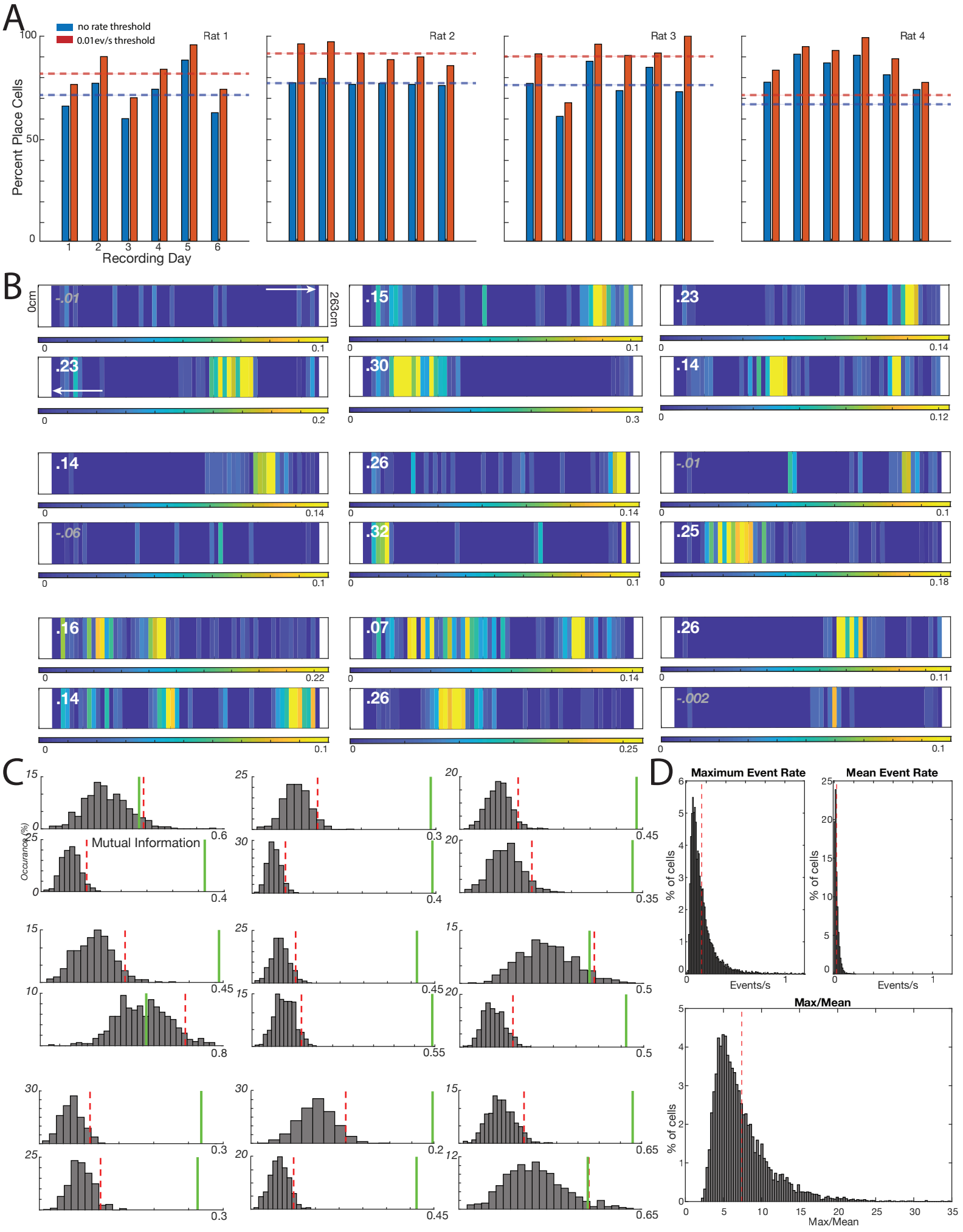
A
no rate threshold
0.01ev/s threshold
Rat 1
Rat 2
Rat 3
Rat 4
Percent Place Cells
Recording Day
B
0cm
263cm
C
Mutual Information
Occurance (%)
D
Maximum Event Rate
Mean Event Rate
% of cells
Events/s
Max/Mean

Figure 5

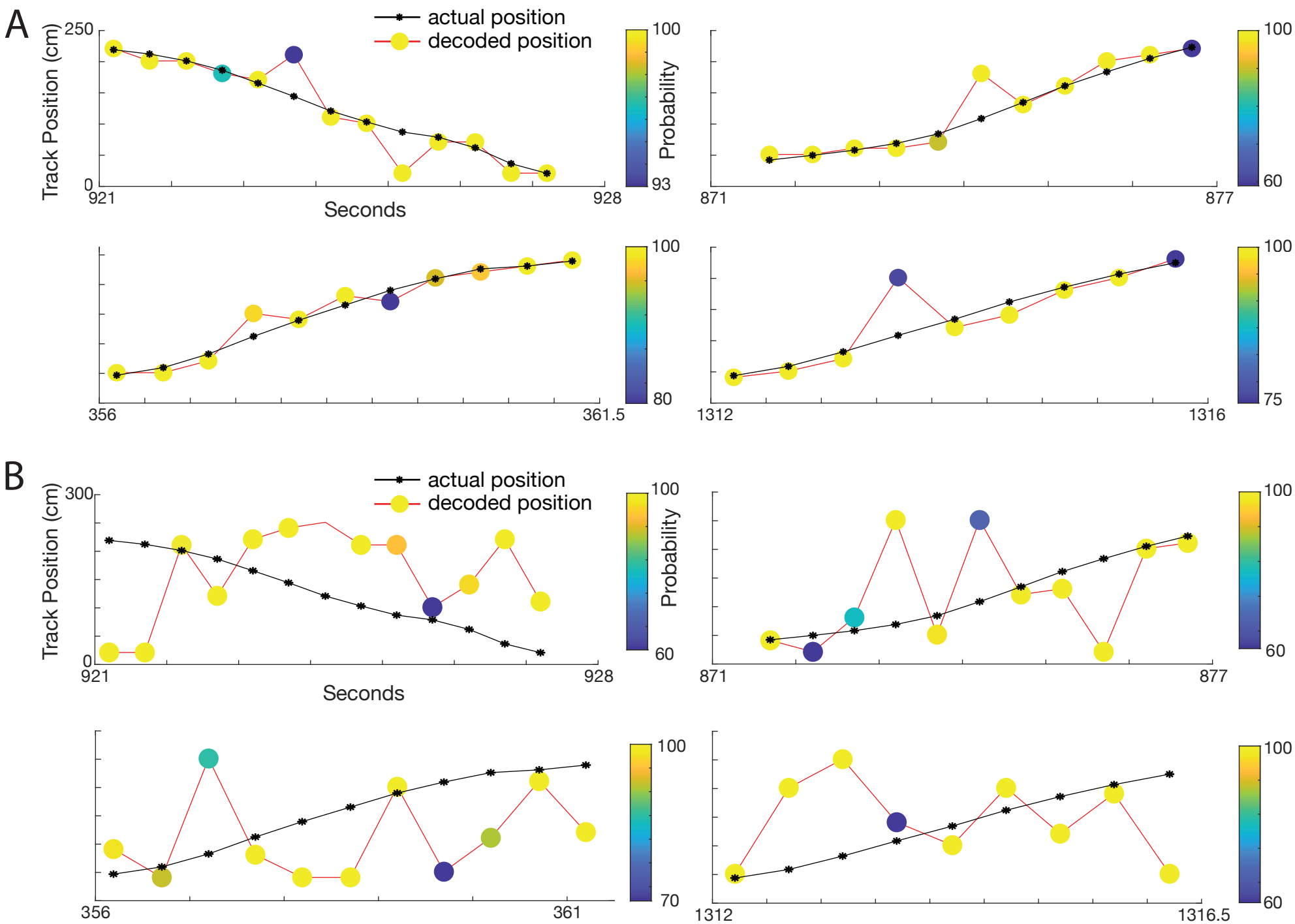
A
actual position
decoded position
Track Position (cm)
250
0
921
928
Seconds
Probability
100
93
871
877
100
60
356
361.5
100
80
1312
1316
100
75
B
actual position
decoded position
Track Position (cm)
300
0
921
928
Seconds
Probability
100
60
871
877
100
60
356
361
100
70
1312
1316.5
100
60

Figure 6

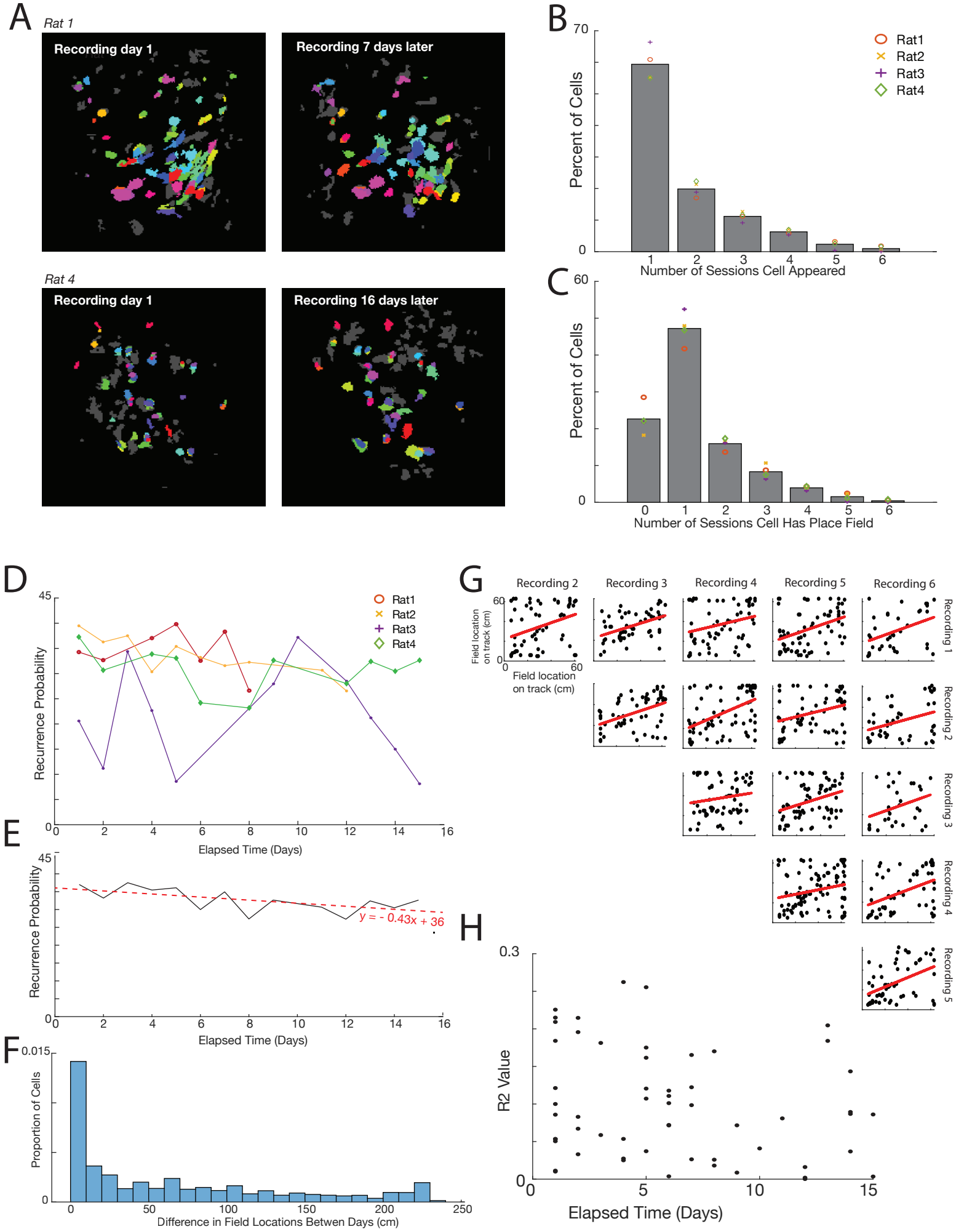
A
Rat 1
Recording day 1
Recording 7 days later
Rat 4
Recording day 1
Recording 16 days later
B
Percent of Cells
Number of Sessions Cell Appeared
Rat1
Rat2
Rat3
Rat4
C
Percent of Cells
Number of Sessions Cell Has Place Field
D
Recurrence Probability
Elapsed Time (Days)
Rat1
Rat2
Rat3
Rat4
E
Recurrence Probability
Elapsed Time (Days)
y = - 0.43x + 36
F
Proportion of Cells
Difference in Field Locations Betwen Days (cm)
G
Recording 2
Recording 3
Recording 4
Recording 5
Recording 6
Recording 1
Recording 2
Recording 3
Recording 4
Recording 5
Field location on track (cm)
Field location on track (cm)
H
R2 Value
Elapsed Time (Days)